Nonlocal effects from boosted dark matter in indirect detection

Kaustubh Agashe,[1] Steven J. Clark,[2] Bhaskar Dutta,[3] and Yuhsin Tsai[1,4]

[1]*Maryland Center for Fundamental Physics, Department of Physics, University of Maryland, College Park, Maryland 20742-4111 USA*

[2]*Brown Theoretical Physics Center and Department of Physics, Brown University, Providence, Rhode Island 02912-1843, USA*

[3]*Mitchell Institute for Fundamental Physics and Astronomy, Department of Physics and Astronomy, Texas A&M University, College Station, Texas 77843, USA*

[4]*Department of Physics, University of Notre Dame, Indiana 46556, USA*

(Received 13 August 2020; accepted 11 February 2021; published 7 April 2021)

Indirect dark matter (DM) detection typically involves the observation of standard model (SM) particles emerging from DM annihilation/decay inside regions of high dark matter concentration. We consider an annihilation scenario in which this reaction has to be initiated by one of the DMs involved being *boosted* while the other is an ambient nonrelativistic particle. This "trigger" DM must be created, for example, in a previous annihilation or decay of a heavier component of DM. Remarkably, boosted DM annihilating into gamma rays at a specific point in a galaxy could actually have traveled from its source at another point in the same galaxy or even from another galaxy. Such a "nonlocal" behavior leads to a nontrivial dependence of the resulting photon signal on the galactic halo parameters, such as DM density and core size, encoded in the so-called "astrophysical" J-factor. These nonlocal J-factors are strikingly different than the usual scenario. A distinctive aspect of this model is that the signal from dwarf galaxies relative to the Milky Way tends to be suppressed from the typical value to various degrees depending on their characteristics. This feature can thus potentially alleviate the mild tension between the DM annihilation explanation of the observed excess of approximately GeV photons from the Milky Way's Galactic Center vs the apparent nonobservation of the corresponding signal from dwarf galaxies.

DOI: 10.1103/PhysRevD.103.083006

I. INTRODUCTION

The search of dark matter (DM) annihilation or decay in experiments designed primarily to detect cosmic-ray particles (such as positrons and antiprotons) and gamma rays, despite being called *indirect* detection of DM, can provide direct information on many properties of DM particles inside galactic halos. For instance, the morphology of the signal shows the DM distribution inside galaxies, and the signal's energy and flux indicate the mass and the interaction strength of DM particles, respectively. Using a novel indirect DM detection scenario, we will illustrate in this work that a comparison of signals from *different* DM halos may even allow us to identify additional details of the generating process.

Over the past few years, several anomalies in astrophysical signatures have provided strong motivations to study such signals from DM models. Among the different searches, the Fermi-LAT experiment [1] produced a gamma-ray survey of the sky for 100 MeV–100 GeV scale photons for both the Milky Way (MW) and dwarf spheroidal galaxies (dSph). The experiment also observed an intriguing excess of gamma rays from the MW center [2] [thus called the Galactic Center excess (GCE)] that has the right morphology to be explained by DM physics [3].[1] As future experiments like e-ASTROGAM [13], Gamma-400 [14], and DAMPE [15] have been proposed to extend the energy coverage of the gamma-ray signal, we expect significant improvements in the observations of MW and dSph. We will therefore use the DM production of gamma-ray signal as an example to discuss how we can probe the dynamics of DM from an ensemble of such detections from different objects.

The differential photon flux $\mathrm{d}\Phi/\mathrm{d}E_\gamma$ arising from DM annihilation or decay in any astrophysical target for indirect DM detection is [16–19]

$$\frac{\mathrm{d}\Phi}{\mathrm{d}E_\gamma} = \frac{\mathrm{d}N}{\mathrm{d}E_\gamma}\begin{cases} \frac{\langle\sigma_{\mathrm{ann}}v\rangle}{8\pi m_\chi^2}\times J_{\mathrm{ann}} & \text{(annihilation)} \\ \frac{1}{4\pi m_\chi \tau_\chi}\times J_{\mathrm{dec}} & \text{(decay)} \end{cases} \tag{1}$$

where the so-called J-factor encodes all the astrophysical contributions. $\mathrm{d}N/\mathrm{d}E_\gamma$ is the photon spectrum produced per

[1]It has also been proposed that unresolved gamma-ray point sources could account for the GCE; see, for example, Refs. [4–6]. For a more recent discussion on this topic, see Refs. [7–12].

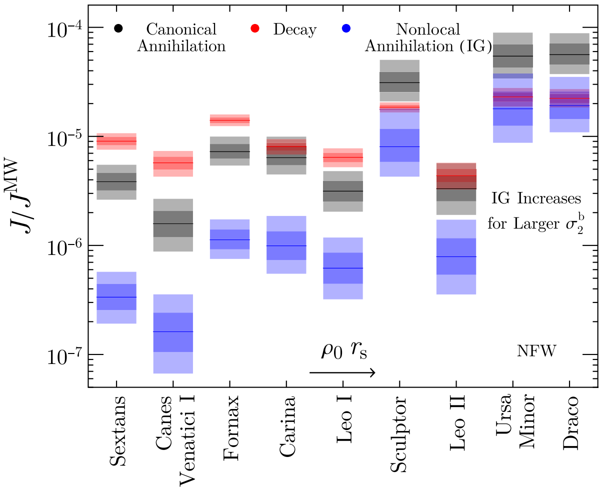

FIG. 1. The ratio of dSph J-factors to the MWs for various dark matter models assuming a NFW DM profile. The dSphs are ordered by increasing values of $\rho_0 r_s$ from left to right. The width of the colored bands at each galaxy represents the 1σ and 2σ uncertainties. DSph NFW profile parameters were obtained from Ref. [16], and their central values are listed in Table I along with those for MW. As MW is used only as a reference here, we take J^{MW} as its central value. σ_2^b is the cross section of the second annihilation process in the nonlocal model; see the text for details. σ_2^b is chosen such that all galaxies have entered the nonlocal regime. The vertical arrow is a reminder that the nonlocal J-factor ratio can be larger for larger cross sections. At its maximum, the J-factor ratio is indistinguishable from canonical annihilation. For the nonlocal annihilation, we only include intragalactic contributions in this figure as noted by IG. Here, the region of interest was taken to be $\theta < 0.5°$ for the dSph and $\theta < 45°$ for MW. The line-of-sight integration extends out to 500 kpc.

annihilation or decay, m_χ is the DM particle mass, $\langle\sigma_{ann} v\rangle$ is the DM's thermally averaged annihilation rate with annihilation cross section σ_{ann}, and τ_χ is the DM lifetime. In the most simple DM scenarios, everything except the J-factor is independent of the galactic environment and originates from the underlying particle physics. For instance, the J-factors for the "canonical" DM annihilation [by which we mean the process of two ambient DM particles annihilating into standard model (SM) particles] and decay that happen in a faraway galaxy at a distance d much larger than the galaxy's size are

$$J_{ann} = d^{-2}\int dV\rho^2(r), \qquad J_{dec} = d^{-2}\int dV\rho(r), \qquad (2)$$

where ρ is the DM density and the integral is performed over the galaxy's volume. The reader can consult Appendix A for a derivation.

Since these J-factors are galaxy dependent, once the gamma-ray signals from different galaxies are measured, we can fit the power of ρ and determine the production mechanism of the signal. As is illustrated in Fig. 1, which

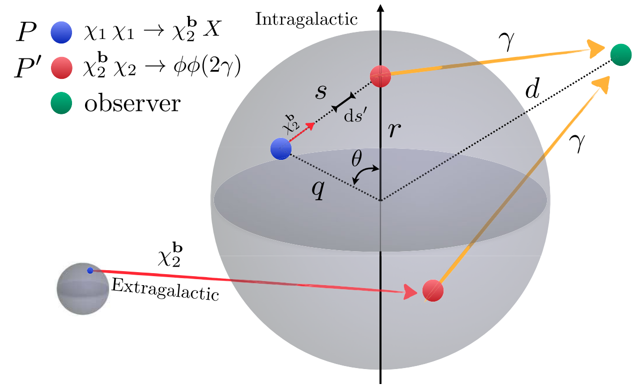

FIG. 2. An illustration of the nonlocal annihilation model. A $\chi_1\chi_1$ annihilation first happens at the blue point P a distant q from the halo's center. The produced χ_2^b travels a distance s and annihilates with a slow-moving ambient χ_2 at the red point P' into ϕ's that decay promptly on galactic scales into gamma rays which are observed at the green point. χ_2^b can also escape their source galaxy and annihilate in another galaxy as noted by the extragalactic arrow.

assumes that DM follows the Navarro-Frenk-White (NFW) distribution [20], the two scenarios of canonical annihilation (black) and decay (red) can be distinguished by their ratio of J-factors with a reference galaxy[2] after taking into account the uncertainty of the NFW fit. We will be using the NFW profile, $\rho(r) = \rho_0(r/r_s)^{-1}(1+r/r_s)^{-2}$, for DM halos throughout this paper; however, many of our qualitative results are valid for other choices of the DM profile. In fact, depending on the process of the gamma-ray production from DM, the indirect detection signal can carry a more complex dependence on galactic parameters, such as DM density and halo size, than in Eq. (2). In this work, we discuss the possibility of bringing in such new galactic dependence in the J-factor using the idea of "nonlocal" annihilation processes, as explained below.

For a schematic framework of nonlocal annihilation, we consider the possibility of a DM interaction occurring at a given point, P, inside the halo first producing a boosted DM particle; see Fig. 2. This boosted particle travels some distance and annihilates with another ambient DM particle producing SM particles at a different location in the galaxy, P', hence dubbed *nonlocal*. As we shall illustrate, due to its mechanism or kinematics, this second annihlation requires the presence of the boosted DM. Not surprisingly, several nonminimal DM models already contain the architecture to include these nonlocal effects. For instance, such an annihilation process can naturally happen in the semi-annihilation model (see, for example, Refs. [21,22]) with

[2]Throughout this work, we take the Milky Way as our reference galaxy; however, the results can be generalized to other choices of reference.

asymmetric DM (ADM) [23] (for a review on ADM, see Ref. [24]) density in which a boosted DM antiparticle (χ^c) is produced at P from a $\chi\chi$ annihilation via the $\chi\chi\chi X$ coupling (where X is an unspecified particle satisfying $m_X \ll m_\chi$). The boosted χ^c later annihilates with a slow moving χ at P' giving SM particles through a coupling that contains $\chi\chi^c$. Note that in ADM models there is no ambient χ^c for initiating this annihilation, thus requiring production from the first interaction to trigger the second. Of course, the interactions that correspond to each annihilation process are still local.

We define the J-factor in the nonlocal process in a manner analogous to canonical annihilation from Eq. (2) with $\sigma_{\rm ann}$ and m_χ substituted for properties of the first annihilation event (σ_1 and m_1). The nonlocal J-factor has additional dependence on the core size and density of the DM halos and the secondary DM annihilation cross section, the latter being part of the intrinsic particle physics. It is noteworthy that the J-factor for the nonlocal model no longer encapsulates *only* astrophysics. This generates another distinct fingerprint in Fig. 1 (blue), with the results depending on an additional product of the galaxy's DM density and size, as we discuss below.[3]

To better illustrate the general concept of nonlocal annihilation, we first present a toy model that generates such a nonlocal annihilation process. The toy model assumes boosted DM production by another heavier DM annihilation process. It is thus a two-component DM model with a two-step annihilation process. This is the nonlocal model shown in Fig. 1. We then discuss the characteristic features of the nonlocal J-factors in galaxies. Finally, we show an application of the nonlocal DM annihilation process for explaining the GCE signal and predicting the corresponding gamma-ray signal from the dSph to be smaller than in the canonical model, consistent with observations, unlike the mild tension in the canonical case. Technical details for the J-factor calculations are given in the Appendixes.

II. DM WITH NONLOCAL ANNIHILATION PROCESSES

We present a concrete toy model that exhibits the properties of nonlocal annihilation which were outlined in the Introduction. We begin with a summary of the general process, followed by a consideration of the motivated parameter space.

In our toy model, we have a heavy component of DM, denoted by χ_1 annihilating into a lighter DM, χ_2; thus the latter is produced with a boost, being therefore labeled with appropriate superscript, $\chi_2^{\rm b}$:

$$\chi_1\chi_1 \to \chi_2^{\rm b} + X. \tag{3}$$

The X particle from the first annihilation can either be another dark sector or an SM particle. In this work, we simply assume X is an invisible particle that does not participate further in any interactions. This first step is followed by $\chi_2^{\rm b}$ annihilating with a stationary χ_2 into another new scalar particle ϕ,

$$\chi_2^{\rm b} + \chi_2 \to 2\phi, \tag{4}$$

which ultimately decays into SM particles, namely, photons in our case:

$$\phi \to 2\gamma. \tag{5}$$

The need for such a mediator between DM and SM will be made clear shortly.

We assume $m_1 \gg m_2$ for the $\chi_{1,2}$ masses, so $\chi_2^{\rm b}$ is relativistic and moves much faster than the escape velocity of the galaxy. We therefore treat all trajectories to be a straight line path; see Fig. 2. For the nonlocal process to be interesting, there is a requirement on the second annihilation cross section, $\sigma_2^{\rm b}$. Once produced, $\chi_2^{\rm b}$ can travel through a typical annihilation length $\ell_{\rm ann} \sim (\sigma_2^{\rm b}\rho_2/m_2)^{-1}$ before annihilating into ϕ's, where ρ_2 is the density of the χ_2 background. To have a gamma-ray signal to detect, we require a significant fraction, greater than or approximately equal to $\mathcal{O}(10\%)$, of $\chi_2^{\rm b}$ to annihilate inside a dSph with radius approximately kpc. Thus, $\ell_{\rm ann}$ should not be much larger than the halo's characteristic size. We therefore need to satisfy

$$\left(\frac{\rho_2}{10\ \mathrm{GeV}\cdot\mathrm{cm}^{-3}}\right)\left(\frac{10\ \mathrm{MeV}}{m_2}\right)\left(\frac{\sigma_2^{\rm b}}{(110\ \mathrm{MeV})^{-2}}\right) \gtrsim 1. \tag{6}$$

Note that in our toy model presented in Eqs. (3)–(5) the peak photon energy is approximately m_1. Therefore, to be within gamma-ray thresholds of the Fermi-LAT experiment, m_1 should be in the range approximately $\mathcal{O}(100\ \mathrm{MeV}\text{–}100\ \mathrm{GeV})$.

To produce large boosts, we require $m_2 \ll m_1$, and thus by our choice of $m_1 \sim \mathcal{O}(100)$ MeV, we are motivated to choose $m_2 \sim \mathcal{O}(10\ \mathrm{MeV})$. The existence of DM particles lighter than 10 MeV usually encounters strong bounds from the cosmic microwave background (CMB) and big bang nucleosynthesis (BBN) measurements (see, e.g., Refs. [31–33]). Some studies nevertheless have suggested the possibility of accommodating sub-MeV scale thermal DM with these constraints. For example, Ref. [32] found that allowing a small fraction (like 10^{-4}) of the DM annihilation into neutrinos as compared to e^+e^-/γ can

[3]Nontrivial galaxy dependent J-factors have been considered in the literature previously, e.g., velocity-dependent DM annihilation [25–27], DM annihilation into mediators which have long-lived decays into SM [28,29], and DM annihilating into its excited state then decays back into the lighter state plus an SM photon [30].

alleviate the $\Delta N_{\rm eff}$ and proton-neutron ratio constraints to allow a sub-MeV DM mass. This can help keep a MeV scale χ_2 without changing the gamma-ray signal significantly. Since our main focus is on the unique feature of gamma-ray signal from the nonlocal annihilation, we will present results for both $m_2 = 10$ MeV and $m_2 = 1$ MeV without specifying the full details of the dark sector that validate the latter case.

The large $\sigma_2^{\rm b}$ cross section required for the second annihilation has two implications. A direct χ_2 annihilation into photons with such a rate would violate millicharged DM bounds (see, e.g., Refs. [34,35] and the references therein). We therefore introduce a singlet mediator ϕ [see Eqs. (3)–(5)] that has a strong coupling to χ_2 and a suppressed coupling to photons. Second, such a large annihilation cross section suggests that χ_2 cannot obtain its relic abundance from a thermal freeze-out process. There are different ways to decouple the χ_2 abundance from its annihilation cross section. For example, in an asymmetric DM scenario, a net $\chi_{1,2}$ abundance versus the antiparticles $\chi_{1,2}^c$ can be produced from an out-of-equilibrium decay of a heavy particle that strongly violates CP symmetry. If the heavy particles were produced from a thermal freeze-out process and have an abundance close to the required DM number density, $\chi_{1,2}$ can obtain the right relic density.[4] After the efficient $\chi_2\chi_2^c$ annihilation depletes χ^c, there is only χ_2 around, and a sizable ρ_2 can be obtained inside halos even for a large $\chi_2\chi_2^c$ annihilation.

To produce the indirect detection signal in such an asymmetric DM scenario, we consider a more specific model where the two DM particles are complex scalars that carry charges $(-1,+2)$ for (χ_1,χ_2) under a dark $\mathrm{U}_d(1)$ symmetry and have the following couplings:

$$\lambda\chi_1\chi_1\chi_2 X + C.c. + y_2|\chi_2|^2\phi^2 + \hat{\lambda}|\chi_2|^4 + \frac{\phi}{f}F_{\mu\nu}F^{\mu\nu}. \qquad (7)$$

To simplify the discussion, we only keep couplings that are relevant to the nonlocal indirect detection signals. The first coupling allows a production of the antiparticle $\chi_1\chi_1 \to \chi_2^* + X$ as in Eq. (3). Here, we consider σ_1 to be similar to the cross section for thermal weakly interacting massive particle (WIMP) DM. Since χ_1 already has the required abundance right after being produced from the out-of-equilibrium decay of a heavy particle [as indicated above, but not explicitly shown in Eq. (7)], χ_1 annihilation with such a rate is never efficient to significantly change its relic density.

The annihilation cross section of $\chi_2^*\chi_2 \to 2\phi$, see Eq. (4), in the center-of-mass frame is

$$\sigma_2 = \frac{\alpha_2}{4m_1m_2} \qquad (8)$$

for $m_\phi \lesssim m_2$. We choose $m_1 \sim \mathcal{O}(100)$ MeV and $m_2 = \mathcal{O}(1\text{–}10)$ MeV, so we need $\alpha_2 = y_2^2/4\pi \sim 1$ to obtain a short enough $\ell_{\rm ann}$ for the gamma-ray signal; see Eq. (6). Motivated by examples in the lattice studies (e.g., Ref. [38]), we take the perturbativity constraint $\alpha_2 \leq 1.2$ in this work. Note that a much heavier χ_1 and χ_2 would need larger α_2, making the theory nonperturbative.

The large y_2 coupling may generate an efficient self-scattering between the ambient χ_2's through a ϕ loop contribution $\frac{\alpha_2}{2\pi}\log\Lambda_{\rm cutoff}$ to the $\hat{\lambda}|\chi_2|^4$ coupling. To satisfy bounds from the various astrophysical constraints, $\sigma_{\chi_2\chi_2\to\chi_2\chi_2}/m_2 = \frac{\hat{\lambda}^2}{64\pi m_2^3} \lesssim 1\ \mathrm{cm^2/g}$ (see Ref. [39] for a review of the bounds), we need the total coupling $\hat{\lambda}_{\rm eff} \approx \hat{\lambda} + \frac{\alpha_2}{2\pi}\log\Lambda_{\rm cutoff} \lesssim (m_2/10\ \mathrm{MeV})^3$. Assuming $\Lambda_{\rm cutoff} \sim 10$ GeV to be larger than all the DM energies we consider, the largest coupling ($\alpha_2 \leq 1.2$) and the lightest χ_2 ($m_2 = 1$ MeV) require a tuning in $\hat{\lambda}_{\rm eff}$ no worse than 0.2%. After being produced from the χ_1 annihilation, the $\chi_2^{\rm b}$ can also scatter with the ambient χ_2 with cross section $\sigma_{\rm scatt} = \frac{\alpha_{\hat{\lambda}}}{4m_1m_2}$ and lose its kinetic energy. If the penetration length $\ell_{\rm pen}$ of losing most of the kinetic energy is shorter than $\ell_{\rm ann}$, we cannot assume $\chi_2^{\rm b}$ to fly in a straight line before the annihilation. However, even if $\chi_2^{\rm b}$ loses most of its energy from a single scattering to χ_2 giving $\ell_{\rm pen} \sim (\sigma_{\rm scatt}n_2)^{-1} = \ell_{\rm ann}(\frac{\alpha_2}{\alpha_{\hat{\lambda}}})$, $\chi_2^{\rm b}$ annihilation still happens well before the particle slows down for the large α_2 we consider.

Finally, ϕ couples to photons, see Eq. (5), via the last term in Eq. (7). In principle, m_ϕ can be larger than m_2 as long as the nonlocal annihilation is kinematically allowed, Eq. (4). However, in the ADM model that we consider here, we need ambient (nonrelativistic) χ_2's to efficiently annihilate into ϕ's to deplete the symmetric part of the χ_2 density; thus, we require $m_\phi < m_2$. When showing examples with $m_2 \lesssim 10$ MeV under this assumption, we need $m_\phi < 10$ MeV, and the allowed f will be tightly constrained by various bounds on the axionlike particle, possibly making ϕ have a decay length comparable to galactic scales. One way to have $m_\phi \sim \mathcal{O}(\mathrm{MeV})$ while making the ϕ's to decay promptly is to consider the cosmological models that can alleviate the $m_\phi - f$ bound in the "cosmological triangle" region, namely, $m_\phi \sim 1$ MeV and $f \sim 10^5$ GeV. For example, as is shown in Ref. [40], the parameters in the cosmological triangle can be allowed either with the presence of $\Delta N_{\rm eff}$, a nonvanishing neutrino chemical potential, or a lower reheating temperature. In this work, we will present results by assuming $m_\phi = 1$ MeV and $f = 10^5$ GeV without discussing the details of the cosmological model. For larger $m_{1,2,\phi}$, the relevant bounds can easily be satisfied under standard cosmology; however, such mass choices will reduce the gamma-ray signal. For the DM mass we consider, the choice of ϕ mass and coupling leads to ϕ decay within 10^{-8} pc after being

[4]A similar setup is discussed in Refs. [36,37] for baryogenesis.

produced. The decay is thus prompt compared to galactic sizes.

Note that the nonlocal behavior of the annihilation still exists even with a smaller coupling and larger (m_2, m_ϕ) that can trivially satisfy the cosmological bounds. Our main motivation for discussing the above scenarios that may require nonstandard cosmology is to relate the nonlocal signal to the known observational sensitivity of the Fermi-LAT experiment. The nonlocal signal from a simpler dark sector can also show up in a different energy scale with a different rate.

III. *J*-FACTOR FROM THE NONLOCAL DM ANNIHILATION

Here, we study the halo dependence of the J-factor for the nonlocal (NL) annihilation process, denoted by J_{NL}. There are two main sources of χ_2^{b} involved in the secondary annihilation. χ_2^{b} can either come from a χ_1 annihilation inside the same halo ["intragalactic" (IG)] or from a χ_1 annihilation in another galaxies ["extragalactic" (EG)]. The two types of signal carry different dependence in DM density. We therefore have

$$J_{\mathrm{NL}} \approx J_{\mathrm{IG}} + J_{\mathrm{EG}} \tag{9}$$

for the nonlocal J-factor. There are also signals coming from χ_2^{b} produced in the intergalactic region, but the signal rate is negligible due to the low DM density outside of galaxies.

In the limit of large σ_2^{b}, J_{NL} is dominated by the intragalactic contribution and reproduces the galactic dependence from the canonical DM annihilation scenario, whereas in the other extreme of small annihilation cross section, both the intra- and extragalactic sources contribute. The intragalactic contribution, J_{IG}, behaves similarly to the canonical DM annihilation with an additional galaxy dependent modulation factor. The extragalactic contribution, J_{EG}, has the galactic dependence of the decay DM scenario. Dominance of intra- versus extragalactic depends on galactic parameters with larger galaxies favoring the intragalactic contribution and vice versa. In this section, we will demonstrate these expected results explicitly. To avoid confusion, we will refer to the J-factors for canonical annihilation and decay, as given in Eq. (2), by J_{ann} and J_{dec}, respectively.

A. Annihilation from intragalactic χ_2^{b}

We first present the expression for J_{IG}, then provide some intuition behind it based on simplifying assumptions. Details of the derivation are given in Appendix B. After first defining the coordinates as in Fig. 2, J_{IG} can be written as

$$J_{\mathrm{IG}} = \int_{\mathrm{ROI}} \mathrm{d}\Omega_{\ell} \int_{\mathrm{LOS}} \mathrm{d}\ell \times \int_{\vec{s}} \frac{\mathrm{d}^3\vec{\hat{s}}}{\hat{s}^2} \frac{\mathrm{d}\mathcal{P}_{\chi_2^{\mathrm{b}}\chi_2}(\hat{r},\hat{s})}{\mathrm{d}\hat{s}} [\rho_{1,0}\eta_1(\hat{q})]^2 \frac{\mathrm{d}N}{\mathrm{d}\Omega_{\vec{s}}}(\vec{\hat{s}},\vec{\ell}). \tag{10}$$

The result contains four components. $[\rho_{1,0}\eta_1(\hat{q})]^2$ gives the number density product between two χ_1 particles that annihilate into χ_2^{b}. This is essentially the source term for χ_2^{b} production. $\mathrm{d}\mathcal{P}/\mathrm{d}\hat{s}$ gives the probability of having χ_2^{b} annihilate after traveling a displacement $\vec{s}$ from the first (χ_1) annihilation point. The $\hat{s}^{-2}$ factor takes into account the geometrical suppression of χ_2^{b} flux that reaches the second annihilation point. Finally, the angular distribution of the signal due to the χ_2^{b} boost in the second annihilation is described by $\mathrm{d}N/\mathrm{d}\Omega_{\vec{s}}$. We perform over a region-of-interest (ROI) and a line-of-sight (LOS) integral for the final result.

To better identify the galaxy-dependent parameters in the expression, we define the dimensionless lengths $(\hat{r},\hat{s},\hat{q}) = (r,s,q)r_s^{-1}$ so that the integral over the lengths is independent of the galaxy's size. In this notation, the $\hat{q}$ is a function of $(\hat{r},\theta,\hat{s})$ as in Fig. 2. We also define $\eta_i(\hat{r}) = \rho_i(r_s\hat{r})/\rho_{i,0}$ to separate the galaxy-dependent properties from the characteristic profile, where i corresponds to $\chi_{i=1,2}$. The annihilation probability

$$\frac{\mathrm{d}\mathcal{P}_{\chi_2^{\mathrm{b}}\chi_2}(\hat{r},\hat{s})}{\mathrm{d}\hat{s}} = \Lambda\eta_2(\hat{r})\exp\left[-\Lambda\int_0^{\hat{s}}\mathrm{d}\hat{s}'\eta_2(\hat{s}')\right] \tag{11}$$

contains a surviving probability of χ_2^{b} that is exponentially suppressed by the distance $\hat{s}$ that χ_2^{b} travels.

$\int \mathrm{d}\hat{s}'$ integrates the annihilation probability χ_2^{b} on its way to the final annihilation point. The probability function is solely dependent on the characteristic density profile and the dimensionless quantity

$$\Lambda \equiv r_s\rho_{2,0}\sigma_2^{\mathrm{b}}/m_2, \tag{12}$$

which is roughly just the inverse of the typical annihilation length (ℓ_{ann}) introduced in the earlier section in units of the halo/core size. In the case of $r_s \ll \ell_{\mathrm{ann}}$, it corresponds to the probability of χ_2^{b} annihilating inside a halo with constant χ_2 density $\rho_{2,0}$ and characteristic size r_s. The exponential factor in Eq. (11) indicates the surviving probability of χ_2^{b} after traveling a distance s to the second annihilation point. As mentioned before, $\mathrm{d}N/\mathrm{d}\Omega_{\vec{s}}$ is the angular distribution of the signal as a result of the second annihilation occurring in a boosted frame and is dependent on the angle between the direction of χ_2^{b}'s momentum, $\vec{r}$, and the observer, $\vec{\ell}$. To write it in the form shown in Eq. (1), we assumed the spectrum does not depend on this angle. This is supported by our assumption discussed later of approximating the angular distribution with a delta function. For a more complete equation including spectral angular dependence, see Appendix B. However, in the limit $d \gg r_s$ where d is the distance the galaxy is away from the observer, this effect can be approximated as effectively isotropic. This isotropy is a result of all points in the galaxy being equally far from the observer, resulting in the various $\chi_2^{\rm b}$ directions averaging out over the final volume integral. In this faraway galaxy approximation,

$$J_{\rm IG} = d^{-2} \int_{\vec{r}} {\rm d}V \int_{\vec{s}} \frac{{\rm d}^3\vec{\hat{s}}}{4\pi\hat{s}^2} \frac{{\rm d}\mathcal{P}_{\chi_2^{\rm b}\chi_2}(\hat{r},\hat{s})}{{\rm d}\hat{s}} [\rho_{1,0}\eta_1(\hat{q})]^2. \quad (13)$$

For detailed calculations of J-factors in this work, we use the full expression Eq. (10) assuming ${\rm d}N/{\rm d}\Omega_{\vec{s}}$ is a delta function in line with $\vec{s}$ due to the high boost of $\chi_2^{\rm b}$ in the second annihilation.

Next, we consider two limiting cases of $J_{\rm NL}$ through Λ in order to understand analytically the morphology of the NL signal versus the canonical annihilation scenario. Recall from Eq. (12) that Λ is effectively the inverse of the free-streaming length of $\chi_2^{\rm b}$ in units of galactic size. This also serves as a useful cross-check.

In the $\Lambda \gg 1$ limit, it is clear that $\chi_2^{\rm b}$ annihilates right after its production from the χ_1 annihilation. The exponential factor in Eq. (11) is non-negligible only for $s \lesssim r_s/\Lambda \ll r_s$. We thus expect the J-factor for the NL model to be proportional to ρ_1^2 as in Eq. (2) for the canonical case. Indeed, by taking the large Λ limit in Eq. (11), since $\lim_{\Lambda\eta_2\to\infty} \Lambda\eta_2 \exp(-\Lambda\eta_2\hat{s}) \approx \delta(\hat{s})$ for $\hat{s} \geq 0$, Eq. (13) recovers the result for the canonical annihilation process:

$$J_{\rm IG} = d^{-2} \int {\rm d}V\rho_1^2(r) \quad (14)$$

On the other hand, when $\Lambda \ll 1$, the exponential factor in Eq. (11) reduces to 1 if we expand the expression to linear order in Λ. It is also convenient to perform the volume integral $\int {\rm d}^3\vec{s}$ in terms of $\int {\rm d}^3\vec{q} \sim 4\pi \int {\rm d}q q^2$. Equation (13) thus reduces to

$$J_{\rm IG} = 4\pi\rho_{1,0}^2 r_s^3 d^{-2}\Lambda \int \hat{r}^2{\rm d}\hat{r}\eta_2(\hat{r}) \int \frac{\hat{q}^2{\rm d}\hat{q}}{\hat{s}^2}[\eta_1(\hat{q})]^2, \quad (15)$$

where the integrals are dimensionless and only depend on the characteristic profile. They are thus identical for all galaxies with the same profiles η_i. Following the assumption of the NFW profile, we can further relate this expression to $J_{\rm ann}$ in the canonical annihilation case. Since the gamma-ray signal is mainly produced in the inner part of the halo (so $\hat{r},\hat{q} \lesssim 1$), the integral gets its dominant contribution when the DM profile is $\eta_1(x) = \eta_2(x) \sim x^{-1}$ for $x = \hat{r}$ or $\hat{q}$. The $\hat{s}$ in the integrand is approximately $\hat{s} \sim \hat{r}$ when $0 \lesssim \hat{q} \lesssim \hat{r}$ and $\hat{s} \sim \hat{q}$ when $\hat{r} \lesssim \hat{q} \lesssim 1$. After performing the d$\hat{q}$ integral for $0 \lesssim \hat{q} \lesssim 1$

TABLE I. Best-fit galactic halo density and radius parameters for various galaxies. The ratios of $\rho_0 r_s$ for each galaxy with the Milky Way are also shown. The DM distribution is assumed to be the NFW profile. Values for the Milky Way are derived using a local density of 0.4 GeV/cm^{-3}, $r_s = 20$ kpc, and our local radius of 8.1 kpc. The dSph values are derived from Ref. [16].

Galaxy	ρ_0 (GeV/cm^{-3})	r_s (kpc)	$\frac{(\rho_0 r_s)^{\rm MW}}{(\rho_0 r_s)^{\rm Gal}}$.
MW	0.345	20	1
Sextans	0.218	2.10	15.1
Canes Venatici I	0.381	1.70	10.7
Fornax	0.359	2.44	7.89
Carina	1.18	0.812	7.22
Leo I	1.13	1.17	5.25
Sculptor	1.74	0.920	4.33
Leo II	2.57	0.636	4.23
Ursa Minor	2.54	0.804	3.38
Draco	2.96	0.728	3.20

and using the relation between DM profiles, we can rewrite the J-factor as

$$J_{\rm IG} \sim \Lambda d^{-2} \int {\rm d}V\rho_1^2(r) \sim \Lambda J_{\rm ann}. \quad (16)$$

The result is rather intuitive since it is the $J_{\rm ann}$ in Eq. (2) that initiates the process from a canonical χ_1 annihilation times a suppression factor Λ that corresponds to the probability of $\chi_2^{\rm b}$ annihilation. Under the same assumption of the NFW profile and the isotropy of the signal, a similar estimate can be done for the MW, and it can be shown that the J-factor is also approximately $\Lambda J_{\rm ann}$ but with Λ derived for the MW halo. Thus, NL annihilation produces an additional $\rho_{2,0}r_s$ dependence via Λ to the J-factor that is not present in the canonical framework. This additional term is a galaxy-dependent modulation to the J-factor. In Fig. 1, we have therefore ordered the dSphs in the horizontal axis by increasing $\rho_0 r_s$; see Table I. As we can see, the variations of the J-factor ratios from canonical annihilation do indeed follow the same ordering.

Traditionally, we can separate the galaxy-dependent factor from the particle physics contribution to the signal rate and define J-factors to be independent of DM physics such as mass and cross section. For the nonlocal model, we define the J-factor as in Eq. (10) so that in the limit of large secondary (or prompt χ_2) annihilation it reproduces the canonical expression with $\sigma_{\rm ann}$ and m_χ in Eq. (1) substituted for properties of the first annihilation event. With this definition of the J-factor, we see that in the opposite limit of a very small cross section [see Eqs. (15)–(16)] $\sigma_2^{\rm b}$ dependence survives via the Λ factor, and the cross section is still separable. However, except in these most extreme cases of Eq. (10) as observed in Eqs. (14) and (15), the secondary annihilation cross section is genuinely inseparable from the astrophysics. This region corresponds to the critical value

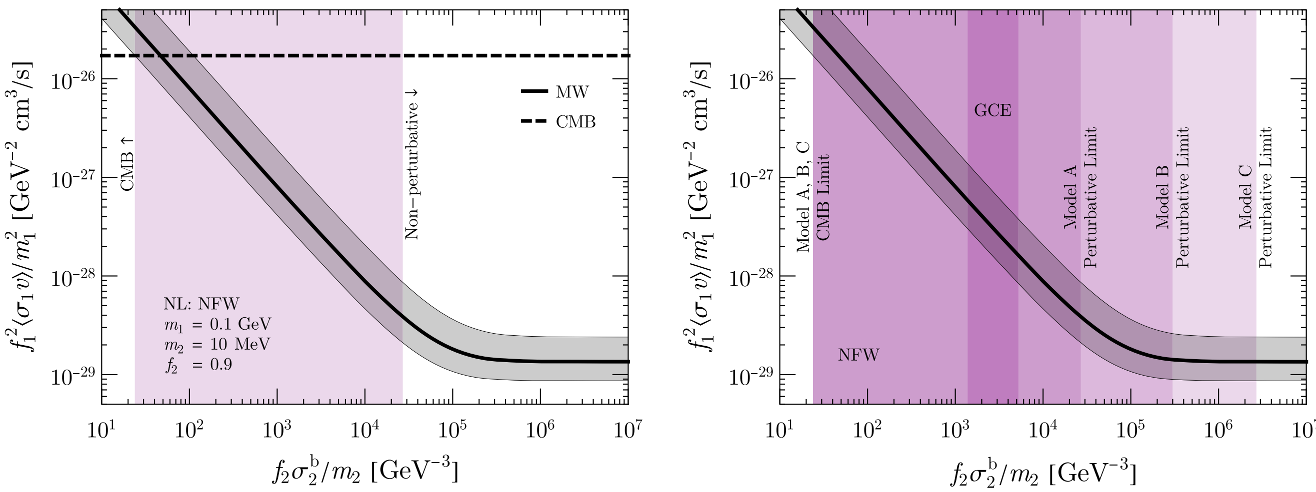

FIG. 3. The χ_1 annihilation rate in the NL model (solid) for producing gamma-ray signals consistent with a fixed flux in the MW for model A (left) and a combined image of all example models (right). The width of the band corresponds to 1σ error bars assuming the local $\rho_{\rm MW} = 0.4 \pm 0.1$ GeV/cm^3 and $r_{\rm Earth} = 8.1$ kpc. The required $\langle\sigma_1 v\rangle$ to fit the flux decreases linearly for $\sigma_2^{\rm b}/m_2$ that is much smaller than the critical value of $\sigma_2^{\rm b}/m_2$ corresponding to $\Lambda \sim 1$; see the text for details. At larger $\sigma_2^{\rm b}/m_2$ where $\Lambda \gg 1$, $\langle\sigma_1 v\rangle$ is constant as the MW exits the nonlocal regime. The CMB upper bound (dashed) on $\langle\sigma_1 v\rangle$ for the model is also shown, and we translate it into a lower bound on $\sigma_2^{\rm b}$ for a fixed flux (the intersection between the solid and dashed curves). Model masses are shown in Table II as benchmark examples. We take $\alpha_2 \leq 1.2$ as the nonperturbativity constraint and set an upper bound on $\sigma_2^{\rm b}$ via Eq. (8). Allowed regions for $\sigma_2^{\rm b}/m_2$ are shaded in purple with the left edge set by violating CMB constraints and the right set by the model becoming nonpertubative.

of $\Lambda \sim 1$ where we transition between these two extreme cases.

In this work, we present numerical results for the four example models described in Table II. Besides the different choices of DM masses, we also keep the fraction of χ_2 density as a variable,

$$f_i \equiv \frac{\rho_{0,i}}{\rho_{0,1} + \rho_{0,2}}, \quad i = 1, 2, \tag{17}$$

and assume both particles follow the same NFW profile in all cases. One can relax the assumption and follow the same analysis as we describe for different DM profiles. In Fig. 3 (left), we show an example of the constraints using model A that can be placed on the NL process described in Eqs. (3)–(5) in the $\sigma_1 - \sigma_2^{\rm b}$ plane by requiring the gamma-ray flux to be constant.[5] We rescale the required annihilation cross sections shown in the axes labels by $f_{1,2}$ and $m_{1,2}$, so the result (black) curve is the same for all the Table II models. This is observed in Fig. 3 (right) where the only difference between the various scenarios is the CMB and the perturbativity constraints. The CMB bound (dashed black line) on the photon injection from χ_2 annihilation assumes the second annihilation is prompt around reionization due to increases in χ_2's density. The CMB bound requires $\langle\sigma_1 v\rangle \lesssim 2 \times 6 \times 10^{-26} (m_1/7\ {\rm GeV})(1 - f_2)^{-2}$ cm^3/ s [41,42]. We therefore set a lower bound on $\sigma_2^{\rm b}/m_2$ by requiring that the lower 1σ error bar on σ_1 needed to fit the flux be below the CMB bound. The factor of 2 and f_2 are a result of rescaling to account for only half of the annihilation energy going into SM particles and a different ρ_1, respectively. For the DM masses we consider, the α_2 coupling in Eq. (8) becomes nonperturbative when $\sigma_2^{\rm b}/m_2 > 3 \times 10^4$ GeV^{-3}; this sets an upper bound on the $\chi_2^{\rm b}$ annihilation. The allowed range of $\sigma_2^{\rm b}/m_2$ is displayed in purple.

The signal in Fig. 3 originates from the MW with an ROI $2° < \theta < 20°$ from the Galactic Center, and we only consider the intragalactic contribution; however, the extragalactic contribution is negligible for the MW as shown later. Note that, even though we use a normalization

TABLE II. DM masses and energy density fraction used in the different example models. The m_1 of the "GCE" case comes from fitting the gamma-ray spectrum to the GCE signal. As discussed in Sec. II, we choose $m_\phi = 1$ MeV in all the examples. We assume the NFW profile $\rho_1/\rho_{1,0} = \rho_2/\rho_{2,0} = [r/r_s(1 + r/r_s)]^{-1}$ for all the models.

Model	m_1 (GeV)	m_2 (MeV)	f_2
A	0.1	10	0.9
B	0.1	1	0.1
C	0.1	1	0.9
GCE	5.68	1	0.1

[5]We require the flux to be described by Eq. (25) with $f_0 = 9.38 \times 10^{-8}$ cm^{-2} s^{-1} sr^{-1} described later in this work. This particular value for f_0 is the best-fit spectral normalization for our toy model to the GCE, which requires $m_1 = 5.68$ GeV.

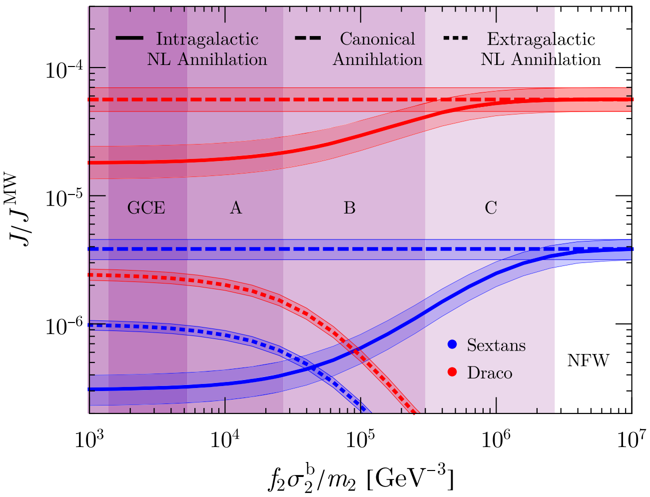

FIG. 4. Ratio of $J/J^{\rm MW}$ for select dSphs. The nonlocal J-factor (solid) is constant at large σ_2/m_2, drops when the dSph enters the nonlocal regime, and then levels out when MW also becomes nonlocal. The canonical annihilation case is also shown (dashed). These two models are the same at large σ_2/m_2 as they are both local. Estimates for the extragalactic nonlocal contribution from each galaxy are also shown (dotted). The bands are 1σ error estimates. The error bars for the extragalactic portion only reflect errors in the second annihilation galaxy and do not include any portion from uncertainties in determining the background $\chi_2^{\rm b}$ flux from the extragalactic sources, which may be large due to both our method for the halo production rate and our treatment of evolution of halo populations and subhalos. We also show the allowed regions due to CMB and nonperturbativity bounds discussed in Fig. 3 using purple for the four models in Table II.

influenced by the GCE to obtain these results, the choice of m_1 for models A, B, and C produces a $E_\gamma^2 {\rm d}N_\gamma/{\rm d}E$ spectrum peaked around 50 MeV and thus cannot explain the GCE; however, the resulting gamma rays are still energetic enough to be potentially observable in the future.

The requirement of the signal flux determines $\langle\sigma_1 v\rangle$ in Fig. 3 as a function of $f_2\sigma_2^{\rm b}/m_2$. The relevant J-factors are calculated by numerically solving Eq. (10) for the galactic signal. As anticipated from Eq. (16), the MW signal for the NL model is linearly suppressed for small $\Lambda = (\rho_{2,0} r_s)\sigma_2^{\rm b}/m_2$, thus necessitating a larger $\langle\sigma_1 v\rangle$ to obtain the required signal rate. The NL suppression no longer applies for $\Lambda \gtrsim 1$, i.e., when $f_2\sigma_2^{\rm b}/m_2 \gtrsim 10^5$ GeV^{-3} for the MW. Thus, the J-factor asymptotes to the canonical DM annihilation as we have discussed, and the required $\langle\sigma_1 v\rangle$ no longer depends on $\sigma_2^{\rm b}/m_2$.

Next, using our toy NL model, we study the signal rate for different dSphs as a function of $\sigma_2^{\rm b}/m_2$. In Fig. 4, we show the ratio of J-factors between dSphs and the MW signals using the same ROI as Fig. 1. The solid and dashed curves are from the nonlocal and the canonical DM annihilations for Sextans (blue) and Draco (red). In the small $\chi_2^{\rm b}/m_2$ annihilation limit, we observe a clear reduction of the ratio between the nonlocal signals compared with their canonical counterpart due to both MW and dSph annihilations suffering a similar $\Lambda \ll 1$ suppression. From the discussion below Eq. (16), the ratio of the J-factors for dSph vs MW is modified in the nonlocal model relative to the canonical by approximately $\Lambda^{\rm dSph}/\Lambda^{\rm MW} = (\rho_{2,0} r_s)^{\rm dSph}/(\rho_{2,0} r_s)^{\rm MW}$. Crucially, $\rho_{2,0} r_s$ is different for each galaxy with the MW being the largest in our local group by a factor of a few, which explains the suppression of J-factor ratios shown in Fig. 4; see Table I. Moreover, this effect varies with the specific dSph in consideration; it is, however, independent of both χ_1 and χ_2 particle parameters. Indeed, as seen in Fig. 4, this dilution is more significant for Sextans because its $\rho_{2,0} r_s$ is smaller than Draco's. This small cross section regime is what is plotted in Fig. 1. The J-factor suppression is clearly seen, and its magnitude decreases as we move horizontally on the figure to larger $\rho_{2,0} r_s$, matching the above expectation.

As already indicated in Fig. 3 for MW, upon increasing $\sigma_2^{\rm b}$, the galaxies start exiting from the NL suppression and become canonical for $\sigma_2^{\rm b}/m_2 \gtrsim 1/(\rho_{2,0} r_s)$. At this scale, the annihilation length of $\chi_2^{\rm b}$ is smaller than the galaxy, and the J-factor eventually asymptotes to the canonical result. This transition from NL to canonical gives rise to interesting features in the ratio of J-factors. Because each galaxy has a different $\rho_{2,0} r_s$, they each transition at a different $\sigma_2^{\rm b}/m_2$. This behavior is directly observed in Fig. 4. The rise in the ratios of J-factors around 10^5 GeV^{-3} corresponds with MW's transition, while the flattening of the ratio around 10^6 GeV^{-3} corresponds to each dSph's transition. Again, note that the particular ordering and scale of the flattening of the J-factor ratio for the two galaxies corresponds to the hierarchy in $\rho_{2,0} r_s$.

Conceptually, it is convenient to consider these two transitions and the three distinct regions they produce with decreasing cross section moving from right-to-left on Fig. 4 in contrast to our earlier discussion, which moved from left-to-right. For large $\sigma_2^{\rm b}/m_2$, we identify the canonical region where both the MW and the dSph are in the $\Lambda \gg 1$ regime; here, their J-factors do not depend on the second particles properties and are thus constants. Note that the ratio merges with the canonical annihilation ratio as expected. As we lower the cross section, because $\rho_{2,0} r_s$ of Sextans is smaller than Draco, Sextans exits the canonical regime at a slightly larger $\sigma_2^{\rm b}/m_2$ than Draco, as seen in Fig. 4. Next, the intermediate region where the galaxy with smaller $\rho_{2,0} r_s$ becomes NL, while the other is still canonical. This results in the J-factor ratio having linear dependence on $\sigma_2^{\rm b}/m_2$ via $\Lambda^{\rm dSph}$. Finally, in the pure NL region where both galaxies are NL, each galaxy has its own Λ dependence. This results in the ratio approximately $(\rho_{2,0} r_s)^{\rm dSph}/(\rho_{2,0} r_s)^{\rm MW}$, independent of $\sigma_2^{\rm b}$, as discussed earlier.

In summary, the intragalactic NL contribution possesses a striking feature as seen in Figs. 1 and 4. For a fixed MW flux, not only is there a suppression of the signal relative to the canonical model for each dSph, but the level of suppression depends on the density and size of the galaxy as well as the $\chi_2^{\rm b}$ annihilation cross section, as shown in Fig. 4.

B. Annihilation from extragalactic $\chi_2^{\rm b}$

Since most of the $\chi_2^{\rm b}$s can escape their source galaxy in the $\Lambda \ll 1$ limit, we should also consider $\chi_2^{\rm b}$ produced in *other* galaxies traveling to and annihilating in a given target galaxy. As we will discuss, the signal produced by extragalactic $\chi_2^{\rm b}$ has a J-factor halo dependence similar to the decay DM scenario, unlike the intragalactic discussed above. The extragalactic signal magnitude is roughly comparable to the intragalactic signal, and either can be the dominant contributor depending on the number of halos in the Universe which produce the extragalactic $\chi_2^{\rm b}$ flux and the characteristics of the target galaxy. Larger galaxies are more likely to be intragalactic dominated due to their large internal $\chi_2^{\rm b}$ production.

We first provide an order of magnitude estimate of the signal rate. We assume the $\chi_2^{\rm b}$ flux to be mainly produced from MW-sized main galaxies (MGs) that are uniformly distributed throughout the whole Universe. We take the average galactic mass to be approximately $8\times10^{11}\ M_\odot$ based on the Virgo Cluster.[6] This mass is near MW's, supporting our $\chi_2^{\rm b}$ estimate. With the average matter density in the Universe[7] $\rho_m = 4.1\times10^{10}\ M_\odot/\ \mathrm{Mpc}^3$, we estimate the average galaxy density $n_{\rm halo}\sim 0.05\ \mathrm{Mpc}^{-3}$.

We assume $\Lambda \ll 1$, and most $\chi_2^{\rm b}$ leave their source galaxy, so the rate of χ_2 annihilation in a nearby "target" galaxy (dubbed TG) that we observe is given by

$$\frac{\mathrm{d}N_{\chi_2}^{\rm ann}}{\mathrm{d}t} \sim \frac{\langle\sigma_1 v\rangle}{2m_1^2}\Phi_{\rm halo}\left[\int \mathrm{d}\bar{V}\,\frac{n_{\rm halo}}{4\pi\bar{r}^2}\right](\pi r_s^2\Lambda)^{\rm TG}. \tag{18}$$

The leading terms in front of the square brackets in general estimate the production rate of $\chi_2^{\rm b}$ and their escape probability from a single main galaxy. Since here we are working in the $\Lambda \ll 1$ limit where most $\chi_2^{\rm b}$'s escape their parent galaxy, it reduces to simply the $\chi_2^{\rm b}$ production rate with

$$\Phi_{\rm halo} \approx \int \mathrm{d}V(\rho_1^{\rm MG}(r))^2. \tag{19}$$

The number density integral in square brackets estimates the total number of halos in the visible Universe with an area suppression which accounts for dilution of $\chi_2^{\rm b}$ flux due to distance from the target galaxy. The final term is the capture cross section of the target galaxy, $(\pi r_s^2\Lambda)^{\rm TG}$, with the physical area multiplied by the probability of capture. The corresponding J-factor can thus be obtained through an ROI and LOS integration: $J_{\rm ann} = \frac{2m_\chi}{\langle\sigma v\rangle_\chi}\int_{\rm ROI}\int_{\rm LOS}\mathrm{d}\ell\mathrm{d}\Omega\frac{\mathrm{d}N_\chi^{\rm ann}}{\mathrm{d}t}$. In the $d \gg r_s$ and $\Lambda \ll 1$ limits,

$$\begin{aligned} J_{\rm EG} &\sim (\pi n_{\rm halo}R(r_s^2)^{\rm TG})\frac{\Lambda^{\rm TG}}{d^2}\int \mathrm{d}V[\rho_1^{\rm MG}(r)]^2 \\ &\sim (\pi n_{\rm halo}R(r_s^2)^{\rm TG})\frac{(\rho_{1,0}^2 r_s^3)^{\rm MG}}{(\rho_{1,0}^2 r_s^3)^{\rm TG}}(\Lambda J_{\rm ann})^{\rm TG}, \end{aligned} \tag{20}$$

where R is the radius of the visible Universe from which $\chi_2^{\rm b}$ originate.[8] We use the usual expression for canonical annihilation $J_{\rm ann}$ from Eq. (2) and simply rewrite the result such that the final set of parentheses is similar to the J-factor estimate from the intragalactic contribution in Eq. (16) for ease of comparison.

The $J_{\rm EG}$ carries an additional suppression relative to the intragalactic contribution of $\pi n_{\rm halo}R(r_s^2)^{\rm TG}\sim 10^{-3}$, where $(r_s)^{\rm TG}\sim$ kpc is the typical size of dSphs and we take $R = 9$ Gpc for the distance back to redshift $z\approx 8$ at the reionization and assume the opacity factor to be 1 [47]. On the other hand, the middle term in Eq. (20) gives an enhancement for a target galaxy smaller than the typical main galaxies. This term originates from the conversion of the galactic volumetric integral which characterizes the $\chi_2^{\rm b}$ production rate from a main galaxy. For dSph, this ratio is of $\mathcal{O}(10^3)$.

Combining all these factors, we see that the resulting $J_{\rm EG}$ is of the same order of magnitude as the intragalactic Eq. (16) for dSphs and subdominant for MG sized galaxies. For extragalactic NL annihilation, since we integrate over the $\chi_2^{\rm b}$ source galaxies in the whole Universe, the only halo

[6]Estimates on the Virgo cluster assume a mass $M_{\rm Virgo} = 1.2\times10^{15}\ M_\odot$ [43] and a galaxy count $N_{\rm Galaxies,Virgo} = 1500$ [44,45].

[7]The average matter density is based on $h = 0.7$ and $\Omega_m = 0.3$.

[8]Note that for $J_{\rm EG}$ calculations the extragalactic volume integration is performed in comoving coordinates. Our constant $n_{\rm halo}$ therefore naturally includes factors related to expansion of the Universe when working in other coordinates. However, we do not include any additional alterations to the halo population. We estimate inclusion of changes to the halo population to be less than an order of magnitude correction to our result due to the growth of virial overdensity as a function of redshift [46,47] as well as using a more rigorous treatment for the halo mass function. Additionally, an interesting outcome of the expansion which we omitted in this calculation is the redshift dependence of $\chi_2^{\rm b}$'s energy, which would result in an altered gamma-ray spectra. In addition, we have omitted substructure considerations to our analysis; however, we estimate it to also at worst introduce an order 1 correction to the J-factor ratios shown in Fig. 4 due to the substructure boost factor (see, e.g., Ref. [48]). This is due to halo concentration, number density, and substructure boost factor dependencies on halo mass competing with each other to produce a near constant $\chi_2^{\rm b}$ production rate per halo mass range. We leave a more detailed analysis of these redshift- and halo-dependent effects to an upcoming work [49].

dependence originates from the target galaxy yielding $J_{\rm EG} \propto \rho_{2,0}/m_2 r_s^3/d^2$, which has similar galactic dependence as the J-factor for decaying dark matter; see Eq. (2).

A more exact calculation of the extragalactic contribution can be derived from Eq. (10) by substituting $(\rho_{1,0}\eta_1)^2 \to n_{\rm halo}\Phi_{\rm halo}$. This substitution alters the production method for $\chi_2^{\rm b}$. Instead of being produced inside the target galaxy, they are now produced uniformly from all space. This simulates an average background of $\chi_2^{\rm b}$s that are produced inside and escape from main galaxies throughout the Universe.

To account for a possible $\chi_2^{\rm b}$ annihilation in the intergalactic medium, $\Lambda\eta_2$ in the exponential of Eq. (11) is replaced with $\Lambda^{\rm InterG}$ where InterG denotes the intergalactic values (note that $\eta_2^{\rm InterG} = 1$) making the integration trivial.[9] With these changes, extragalactic J-factor becomes

$$J_{\rm EG} \approx R_{\rm eff} n_{\rm halo}\Phi_{\rm halo}\left(\frac{\Lambda}{r_s}\right)^{\rm TG}\int_{\rm LOS}\int_{\rm ROI} d\ell d\Omega \eta_2^{\rm TG}(\hat{r}) \tag{21}$$

with

$$R_{\rm eff} = \ell_{\rm ann}^{\rm InterG}(1 - e^{-R/\ell_{\rm ann}^{\rm InterG}}), \tag{22}$$

where $\ell_{\rm ann}^{\rm InterG} = m_2/(\sigma_2^{\rm b}\rho_2^{\rm InterG})$ is the typical annihilation length in the intergalactic medium and R is the same from Eq. (20). $R_{\rm eff}$ originates from $\chi_2^{\rm b}$ suppression due to intergalactic annihilations integrated over the entire volume. In the limit that omits intergalactic annihilations, $R_{\rm eff}$ becomes R. Furthermore, by taking $\ell_{\rm ann}^{\rm InterG} \gg R$, we recover the estimate from Eq. (20) up to the cross section with $(\pi r_s^2)^{\rm TG}$ becoming $\int dV(\eta_2(\hat{r})/r_s)^{\rm TG}$ in the $d \gg r_s$ limit. This variation in the cross section is expected as all paths through the galaxy are not of equal thickness. For larger cross sections, we calculate $\Phi_{\rm halo}$ numerically by $\Phi_{\rm halo} = d^2(J_{\rm ann} - J_{\rm IG})$ in the $d \gg r_s$ limit.

In Fig. 4, we also present the J-factor ratios for the extragalactic contribution. The contribution is comparable to the intragalactic contribution, dominating slightly for Sextans and subdominant for Draco. The dip at $\sigma_2^{\rm b}/m_2 \sim 10^5\ {\rm GeV}^{-3}$ is due to fewer $\chi_2^{\rm b}$ escaping from their source galaxy as observed by the simultaneous transition in the $(J/J^{\rm MW})_{\rm IG}$.

One effect we have not taken into account is the blocking of the external χ_2 flux due to the presence of other galaxies. Although we take the escaping probability $\exp[-\Lambda\eta_2(\hat{r})] \sim 1$ in the small Λ limit, this assumption can fail if χ_2's fly across many galaxies. To see this is not actually the case, we can calculate the solid angle in the sky that is occupied by Milky Way size galaxies (assuming core radius $r_s \sim 10$ kpc). A single galaxy that is $\hat{r}$ away from us covers a fraction of the sky approximately $\frac{\pi r_s^2}{4\pi\hat{r}^2}$. The total fraction of the sky being covered by all galaxies is

$$\int d\hat{r} 4\pi\hat{r}^2 n_{\rm halo}\frac{r_s^2}{4\hat{r}^2} \sim 0.1. \tag{23}$$

This means χ_2 produced in one galaxy only has a 10% chance to hit another galaxy before reaching the target galaxy. Thus, when the escaping probability in each galaxy is close to 1, this blocking does not change the χ_2 flux significantly.

Besides creating the extragalactic signal thus far discussed, these extragalactic $\chi_2^{\rm b}$ can also annihilate with χ_2 outside of galaxies and generate the isotropic gamma-ray background (IGRB) that is also measured by the Fermi-LAT experiment [50]. This signal is produced by the intergalactic annihilations discussed in the context of Eq. (21) and can be simply derived by taking Eq. (21) with the intergalactic medium as the target. The generated IGRB flux is

$$\begin{aligned}\frac{d\Phi_\gamma^{\rm IGRB}}{dE_\gamma d\Omega} &\sim \frac{n_{\rm halo}}{8\pi}\frac{\langle\sigma_1 v\rangle}{m_1^2}\Phi_{\rm halo}R(1 - e^{-R/\ell_{\rm ann}^{\rm InterG}})\frac{dN}{dE_\gamma} \\ &\sim \frac{1.5\times 10^{-9}}{{\rm cm}^2\,{\rm s\,sr}}\left(\frac{\rho_0^2 f_1^2\langle\sigma_1 v\rangle/m_1^2}{10^{-29}\ {\rm cm}^{-3}\,{\rm s}^{-1}}\right)(1 - e^{-R/\ell_{\rm ann}^{\rm InterG}})\frac{dN}{dE_\gamma},\end{aligned} \tag{24}$$

where ρ_0 is the characteristic density of MG and we have assumed $r_s^{\rm MG} = 20$ kpc. Interestingly, the result does not depend on χ_2's properties except in the exponential suppression, which will be minimal when this effect may be important ($\Lambda^{\rm MG} \ll 1$). The parameters used in Table II produce a peak flux $E_\gamma^2 d\Phi_\gamma^{\rm IGRB}/dE_\gamma d\Omega \approx 3\times 10^{-8}\ {\rm GeV\,cm^{-2}\,s^{-1}\,sr^{-1}}$. Comparing the flux with the IGRB bound $E_\gamma^2 d\Phi_\gamma^{\rm IGRB}/dE_\gamma d\Omega \lesssim 10^{-7}\ {\rm GeV\,cm^{-2}\,s^{-1}\,sr^{-1}}$ derived in Ref. [51] for a similar gamma-ray spectrum, our signal should be well within the current constraint (especially once additional cosmological factors are taken into account as discussed above). Nevertheless, this diffuse gamma-ray background is a generic signature of the nonlocal annihilation model, and future experiments may be sensitive to it.

Additionally, producing $\chi_2^{\rm b}$ through χ_1 annihilation in the intergalactic medium is also feasible. However, since the average number density of DM particles in the intergalactic medium is approximately 10^{-5} smaller than in the galaxies, even if the volume of the observable Universe is approximately 10^6 times larger than the sum of main galaxies, such $\chi_2^{\rm b}$ production is negligible.

[9]Note that, even though $r_s^{\rm InterG}$ from $\Lambda^{\rm InterG}$ has no physical connection to the target galaxy, it should remain as $r_s^{\rm TG}$ in order to maintain a consistent definition for the dimensionless integration variables; see the discussion below Eq. (10).

IV. RECONCILING THE GCE AS A SIGNAL OF DM WITH DSPH CONSTRAINTS

Since the nonlocal annihilation process suppresses the dSph gamma-ray signal relative to the signal from the MW comparative to canonical annihilation, an application of the nonlocal annihilation is to explain the potential mild tension between the DM explanation of the GCE signal [3] and the null result in dSph observations (see, e.g., Refs. [52,53]). Note that, while this discrepancy may not be very significant [54], we discuss it here simply as an illustrative application of a specific NL model. The NL mechanism, however, is much broader and is independent of this particular result.

For canonical annihilation, a dSph signal produced by the same process can have a tension that is up to 2σ level for some annihilation channels [55–57]. If we take the tension seriously, the dSph signal needs to be suppressed by less than an order of magnitude in order to satisfy the bound. As we will show, the mild tension can be naturally addressed by the Λ factor in NL annihilation. Additionally, the nonlocal signals with the distinct *fingerprints* in Fig. 1 are only lower than the canonical annihilation signals by a factor of a few; they are thus still within the sensitivity of future observations.[10]

In the right panel of Fig. 3, the model labeled "GCE," see Table II, shows the required $\langle\sigma_1 v\rangle$ for explaining the GCE via Eqs. (3)–(5). We obtain the energy spectrum of the photons by numerically convolving the analytically calculated spectra of ϕ particles from the annihilation and the boosted spectra of an isotropic decay of ϕ into photons. Although the signal comes from a monochromatic decay, $\phi \to 2\gamma$, in ϕ's rest frame, since ϕ has a broad energy distribution from the $\chi_2^b\chi_2$ annihilation, the dN_γ/dE_γ also has a rather smooth spectrum.

We follow the technique outlined in Ref. [55] for calculating the χ^2 statistic for fitting to the GCE.[11] As noted in Ref. [55], the best-fit parameters may not visually appear to be optimal due to large cross-correlations between individual bins. The reduced χ^2 for our model is 2.03 compared with 1.08 (1.52) for canonical $b\bar{b}$ ($\tau\bar{\tau}$) annihilation obtained in Ref. [55] with 22 d.o.f. While the significance for this toy model is weaker than other more standard models, it is used here solely as an example of the behavior rather than a claim to fit the GCE. We obtain the best fit of the GCE signal with the spectrum as shown in Fig. 5 with $m_1 = 5.68$ GeV. For comparison, we also show the best-fit spectra for canonical $\chi\chi \to b\bar{b}$ and $\chi\chi \to \tau\bar{\tau}$ annihilation. The result has only a mild dependence on $m_{2,\phi,X}$ as long as $m_1 \gg m_{2,\phi,X}$. For concreteness, we take $m_2 = m_\phi = m_X = 1$ MeV for the analysis. For a single set of model masses, the fitting routine has one additional free normalization parameter f_0, such that the observed flux from the GCE is

$$\frac{\Phi_{\rm GCE}}{\Delta\Omega_{\rm ROI}} = f_0 \int_{E_{\rm min}}^{E_{\rm max}} \frac{dN\gamma}{dE_\gamma} dE_\gamma. \quad (25)$$

For each value of a set of m_1 with fixed $m_{2,\phi,X}$, we optimized f_0 to produce the minimum χ^2. We then compared all the χ^2s to find the global best fit m_1. Comparing with Eq. (1) and making proper conversions, it is obvious that for NL annihilation

$$f_{0,\rm NL} = \frac{\langle\sigma_1 v\rangle}{8\pi m_1^2} \times \frac{J_{\rm NL}}{\Delta\Omega_{\rm ROI}}. \quad (26)$$

f_0 is thus equivalent to the observed event rate per solid angle and is used to place constraints on $\langle\sigma_1 v\rangle$ in Fig. 3. We take the ROI to be $2° < \theta < 20°$ from the Galactic Center where we have omitted the $\theta < 2°$ as in Ref. [55].

As before, constraints on the photon injection around recombination set an upper bound on $\langle\sigma_1 v\rangle$ via CMB measurements. Together with the bound from keeping α_2 in

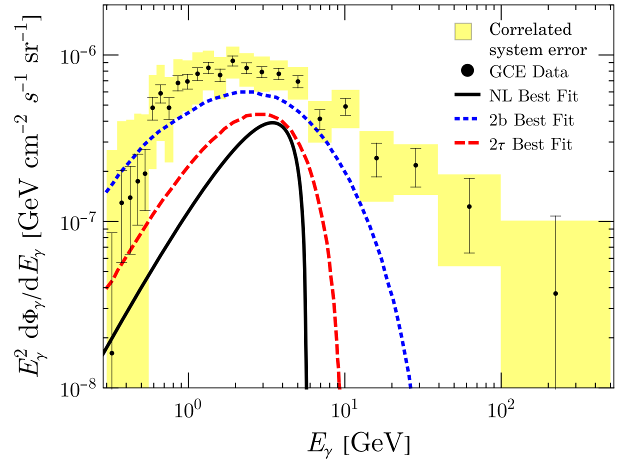

FIG. 5. Best-fit gamma-ray spectrum for our toy model $\chi_1\chi_1 \to \chi_2^b X, \chi_2^b\chi_2 \to 2\phi, \phi \to 2\gamma$. In the fit, most masses were fixed $m_2 = m_\phi = m_X = 1$ MeV. These produced a best-fit value of $m_1 = 5.68$ GeV. Note that for $m_1 \gg m_{2,/,\phi,X}$ the spectrum is largely independent of $m_{2,/,\phi,X}$. For comparison, the best fits for the canonical $b\bar{b}$ (dotted blue line) and $\tau\bar{\tau}$ annihilations (dashed red line) are also shown.

[10] Some other possible solutions to resolve this mild tension have been proposed in literature. For instance, in Ref. [58], the dSph signal is suppressed due to the p-wave DM annihilation process. In Ref. [59], the gamma-ray signal comes from the interaction between interstellar radiation and charged particles produced from the DM annihilation. These scenarios, however, predict much smaller dSph signals that are well below future observational sensitivity.

[11] We use their covariance matrix with our predicted spectra $\chi^2 = \sum_{ij} (\frac{d\bar{N}}{dE_i}(\boldsymbol{\theta}) - \frac{dN}{dE_i})\Sigma_{ij}^{-1}(\frac{d\bar{N}}{dE_j}(\boldsymbol{\theta}) - \frac{dN}{dE_j})$, where dN/dE_i is the measured flux, $d\bar{N}/dE_i(\boldsymbol{\theta})$ is the predicted flux with input parameters $\boldsymbol{\theta}$, and Σ_{ij} is the correlated covariance matrix.

Eq. (8) perturbative, we find a window $1.7\times10^3 < \sigma_2^{\rm b}/m_2 < 3.3\times10^3\ \text{GeV}^{-3}$ for which NL $\chi_2^{\rm b}$ annihilations can produce a sufficient signal to explain the GCE. Based on the differences observed between the NL and canonical signals observed in Fig. 4, we therefore expect a factor of $\approx 3(15)$ suppression for NL over canonical annihilation in the dSph/MW signal comparison. Thus, the suppression is enough to explain the absence of gamma-ray excess from the existing dSph observations, while suggesting that dSph signals can still be observed in the future.

V. CONCLUSION

In this paper, we have explored the scenario where the indirect detection signal comes from two consecutive DM annihilations. The boosted DM produced from the first annihilation can travel a long distance before annihilating with another at-rest DM particle into gamma rays. This means the production of indirect detection signals becomes nonlocal with respect to the first annihilation. In fact, signals from a galaxy can arise either from boosted DM particle production and annihilation in the same galaxy (intragalactic) or be triggered by boosted DM particles coming in from different, faraway, galaxies (extragalactic).

A robust consequence of the nonlocal annihilation is that the J-factor of the gamma-ray signal is different from those of the canonical DM annihilation and decay due to a further dependence on the DM density and size of the halo and an added dependence on the particle physics of the second annihilation. This implies that the associated "ratio of ratios" (the ratio of the signal between two galaxies, say dSph vs MW, as well as a comparison between the nonlocal and canonical models) will actually vary between galaxies. The nonlocal modification is thus galaxy dependent. As we show in Fig. 1, if DM distributions in these dSphs follow the NFW distribution, we will be able to distinguish different DM scenarios once we see the gamma-ray signal from an ensemble of galaxies. We expect a nontrivial galaxy-dependent J-factor can show up in other DM models. For example, in scenarios that have DM annihilation into long-lived particles and later decay into gamma rays [28,29], the corresponding J-factor will be dependent on the lifetime of the long-lived particle and the region of interest around the target galaxy in the observation. The signal can therefore have a different galaxy dependence to our model. The information from the ensemble of galaxies then provides us a chance to distinguish these different processes of signal generation.

The magnitude of this effect on the ratio of ratios heavily depends on the second annihilation cross section; see Fig. 4. Indeed, in the extreme case of a very large DM annihilation cross section, requiring masses below $\mathcal{O}(10)$ MeV scale and/or couplings near the perturbative limit, the nonlocal model mimics the canonical scenario, whereas it is when the annihilation is less efficient that the J-factor ratio for the nonlocal model differs from the canonical model. However, in this opposite limit of a much smaller annihilation cross section, the ratio of J-factors will actually be independent of the annihilation cross section. In this case, the effect still carries additional galaxy dependence as compared to canonical annihilation. This is the case observed in Fig. 1. We thus obtain a prediction for the J-factor ratios for the nonlocal model based on only galactic parameters. It is important to point out that in the "intermediate" regime of annihilation cross sections the ratio of J-factors also depends on the cross section, providing a means for measuring this annihilation rate.

The nonlocal annihilation process not only generates distinct galaxy-dependent signals but can also reconcile the mild tension between gamma-ray signals from the MW and dSphs, namely, explaining the DM annihilation interpretation of the GCE and the null result from dSph. The crucial observation is the gamma-ray signal from dSphs compared with the MW is smaller in the nonlocal scenario than it is for canonical annihilation, thus explaining the lack of dSphs gamma-ray signals in the current observation. However, unlike the explanation in Refs. [58,59], the suppression of the dSph signal from the nonlocal process is only by a factor of a few and would be detectable with slight sensitivity improvements in dSph measurements.

Here, we present some additional examples for future work [49]. While in this work we have discussed the signal using a specific asymmetric DM model with NFW profiles, there are many other scenarios that give the nonlocal annihilation as long as the DM sector produces boosted particles that have a large annihilation cross section with the ambient DM, but the same annihilation process has not been able to deplete the DM density. For example, the nonlocal annihilation process may also happen in a forbidden DM setup [60,61]. Similar to the model in Eqs. (3)–(5) but with $m_\phi > m_2$, the relic abundance of both χ_2 and χ_2^* can be maintained due to the kinematic barrier even with a large $|\chi_2|^2\phi^2$ coupling. However, this barrier is overcome by the boosted DM. In this case, the nonlocal annihilation comes from $\chi_1\chi_1^* \to \chi_2^{\rm b}\chi_2^{\rm b*}$ and $\chi_2^{\rm b}\chi_2^* \to 2\phi(2\gamma)$. Moreover, although we assume the X in Eq. (3), which produces the boosted dark matter, to be an invisible particle for simplicity, X can also be the ϕ particle that generates other gamma-ray signals at a different location from the $\chi_2^{\rm b}$ annihilation. This generates another interesting profile of the gamma-ray signal. Additionally, most of our discussion has focused on producing a gamma-ray signal; however, another source of comparison would be between neutrino production rates and the observed astrophysical neutrino flux [62]. As stated before, we concentrated in this work on the NFW profile. Qualitatively, other profiles, for example the cored Burkert profile [63], exhibit the same NL features because they are due to $\chi_2^{\rm b}$ escaping from their parent galaxy. However, each profile's signal will possess different radial dependencies as well as a different allowed parameter space.

Finally, while a GCE explanation is intriguing and is certainly possible with DM mass of several GeV, in our model, in order to naturally generate a nonlocal signal, the boosted DM should have energy below 100 MeV, and the resulting gamma-ray signal can be close to the threshold of the Fermi-LAT experiment. However, future proposals such as the e-ASTROGAM experiment are designed to cover the less-explored 1–100 MeV gamma-ray region and can better probe nonlocal signals.

To conclude, the nonlocal framework is a natural outcome of multiple extended dark matter models and predicts additional galaxy dependencies in annihilation signals. This additional dependence results in smaller galaxies having an even smaller signal compared with larger counterparts. The comparison between the nonlocal behavior and the canonical framework for different galactic parameters stretches from a maximal difference to naturally merging with the canonical.

ACKNOWLEDGMENTS

We would like to thank Patrick Fox, Cara Giovanetti, Roni Harnik, Dan Hooper, Rebecca Leane, Louis Strigari, Yue Zhang, and Jure Zupan for useful discussions. K. A. and Y. T. were supported in part by the National Science Foundation under Grants No. PHY-1620074 and No. PHY-1914731; the Fermilab Distinguished Scholars Program; and the Maryland Center for Fundamental Physics. S. J. C. was supported by the Brown Theoretical Physics Center. B. D. was supported in part by DOE Grant No. DE-SC0010813. Y. T. was also supported in part by the US-Israeli BSF Grant No. 2018236. Y. T. thanks the Aspen Center for Physics, which is supported by National Science Foundation Grant No. PHY-1607611, where part of this work was performed. K. A. and B. D. would like to thank the organizers of the "2018 Santa Fe Summer Workshop in Particle Physics" where the ideas leading to this work were initiated.

APPENDIX A: ALTERNATE FORMS OF THE J-FACTOR

The J-factors are written in multiple forms, making use of various assumptions throughout the text; in this Appendix, we derive these simplifications. Similar derivations have been included in other works [18,64], and we perform them here for convenience. The differential flux from an interaction seen by an observer is commonly written as Eq. (1). It can also be compactly written for different interaction types as

$$\frac{\mathrm{d}\Phi_\phi}{\mathrm{d}E} = \frac{1}{4\pi}\int_{\mathrm{ROI}} \mathrm{d}\Omega_\ell \int_{\mathrm{LOS}} \mathrm{d}\ell \frac{\mathrm{d}N(r)}{\mathrm{d}V\mathrm{d}t}\frac{\mathrm{d}N_\phi}{\mathrm{d}E}, \tag{A1}$$

where ϕ is just a product from the interaction. The integral is taken over the LOS and ROI observed. $\mathrm{d}N(r)/\mathrm{d}V\mathrm{d}t$ is the interaction rate per unit volume and time. $\mathrm{d}N_\phi/\mathrm{d}E$ is the spectrum of ϕ from the interaction. This form assumes that the interaction is spherically symmetric. As mentioned in the text, Eq. (A1) is typically separated into two parts, namely, the astrophysical and the particle physics parameters. For canonical annihilating dark matter, Eq. (A1) can be written identically to Eq. (1) using

$$J_{\mathrm{ann}} = \frac{2m_\chi^2}{\langle\sigma_{\mathrm{ann}}v\rangle}\int_{\mathrm{ROI}} \mathrm{d}\Omega_\ell \int_{\mathrm{LOS}} \mathrm{d}\ell \left(\frac{\mathrm{d}N(r)}{\mathrm{d}V\mathrm{d}t}\right)_{\mathrm{ann}} \tag{A2}$$

with

$$\left(\frac{\mathrm{d}N(r)}{\mathrm{d}V\mathrm{d}t}\right)_{\mathrm{ann}} = \frac{\langle\sigma_{\mathrm{ann}}v\rangle}{2m_\chi^2}\rho_\chi^2(r), \tag{A3}$$

where χ is the dark matter particle with mass density ρ_χ. A similar expression can be written for decay. For a general expression, it is convenient to define

$$J = \int_{\mathrm{ROI}} \mathrm{d}\Omega_\ell \int_{\mathrm{LOS}} \mathrm{d}\ell f(r), \tag{A4}$$

where $f(r)$ is a scaled version of the number density of events per time which generates the signal, $\mathrm{d}N/\mathrm{d}V\mathrm{d}t$. This scaling is performed in such a way as to remove all possible particle physics contributions. We assume $f(r)$ is a spherically symmetric function centered at $\vec{\ell} = (d, 0, 0)$ in the ℓ coordinate system. In the canonical case, $f(r)$ is $\rho_\chi^2(r)$ for annihilation and $\rho_\chi(r)$ for decay.

1. J-factor in the $d \gg r_s$ limit

The J-factors shown in Eq. (2) assume the observer is far from the galaxy, $d \gg r_s$, such that all points in the galaxy can be treated as at equal distance. To demonstrate this far distance approximation, we restore some of the simplifications to the volume integral in Eq. (A4); this produces

$$J = 4\pi \int \frac{\mathrm{d}V_\ell}{4\pi\ell^2} f(r). \tag{A5}$$

For simplicity, we assume that we have captured all of the signal from the galaxy and have thus taken the integration over the volume of all space. $\mathrm{d}V_\ell$ indicates the integral is performed with ℓ coordinates. The $1/4\pi\ell^2$ is a result of an area suppression of flux with distance. The volumetric integral can easily be shifted to a new coordinate system centered at r, leading to

$$J = \int \frac{\mathrm{d}V_r}{\ell^2} f(r). \tag{A6}$$

Finally, because the profiles have a cutoff scale $r_{\mathrm{cutoff}} \sim r_s$ and $d \gg r_s$, the integral is dominated by the region where $r \ll d$ and thus $|\vec{\ell}| = |\vec{d} - \vec{r}| \approx |\vec{d}|$. This results in the simplification quoted in Eq. (2). Note that a cutoff scale must be imposed for decay with a NFW profile because at arbitrarily large distances its volumetric integral is logarithmically divergent. In this work, we achieve this through our choice of boundaries in our ROI and LOS integrations for computational convenience. Tests showed that this method resulted in percent-level differences from the more traditional method of cutting off at the virial radius. We can also write in this limit the J-factors in the dimensionless integral format as defined in this work,

$$J_{\rm ann} = \frac{\rho_0^2 r_s^3}{d^2} \int \mathrm{d}^3\hat{r}\eta^2(\hat{r}), \tag{A7}$$

$$J_{\rm dec} = \frac{\rho_0 r_s^3}{d^2} \int \mathrm{d}^3\hat{r}\eta(\hat{r}). \tag{A8}$$

APPENDIX B: $J_{\rm NL}$ DERIVATION

In this Appendix, we derive the J-factors and associated functions that arise from the nonlocal annihilation framework, primarily focusing on models where the boosted DM is produced via another annihilation within the same galaxy. In a model where the observed dark matter signal is produced through a secondary interaction, the two interaction events do not necessarily need to occur at the same location in space. Let us consider a two-component dark matter annihilation model with particles χ_1 and χ_2. The annihilation of χ_1 produces a boosted χ_2 referred to from here on as $\chi_2^{\rm b}$. Because of the current conditions, χ_2 is unable to annihilate with itself, but it can annihilate with $\chi_2^{\rm b}$. The general model setup is that one set of dark matter, χ_1, annihilates into another variety, χ_2, but with a nonzero velocity, $\chi_2^{\rm b}$. The boosting allows it to access otherwise forbidden channels; depending on the cross section, $\chi_2^{\rm b}$ may annihilate at a different location from its creation.

For the discussion that follows, we assume all annihilations occur within a galaxy. Subscripts 1 and 2 correspond to the various parameters for particles χ_1 and χ_2, respectively.

1. $\chi_2^{\rm b}$ survival probability

Before calculating the spatial distribution of the $\chi_2^{\rm b}\chi_2$ annihilation, let us derive the probability function $\mathrm{d}\mathcal{P}(r,s)/\mathrm{d}s$ of having a $\chi_2^{\rm b}$ being produced at $s = 0$ (from the χ_1 annihilation) and annihilating at a distance s away; see Fig. 6.

Let us first assume the number density of χ_2 is constant, $n_2(s) = n_2$. When slicing the distance s into infinitesimally small pieces of length Δs, the probability of having $\chi_2^{\rm b}$ to not have annihilated after traveling s but annihilated before $s + \Delta s$ can be written as

$$\begin{aligned}\Delta\mathcal{P}(s) &= (1 - n_2\sigma_2^{\rm b}\Delta s)^{\frac{s}{\Delta s}}(n_2\sigma_2^{\rm b}\Delta s),\\ &= \exp\left[\frac{s}{\Delta s}\ln(1 - n_2\sigma_2^{\rm b}\Delta s)\right](n_2\sigma_2^{\rm b}\Delta s)\\ &\approx e^{-n_2\sigma_2^{\rm b}s} n_2\sigma_2^{\rm b}\Delta s,\end{aligned} \tag{B1}$$

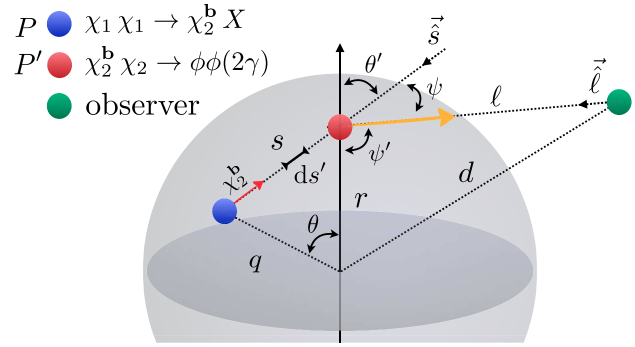

FIG. 6. A modified version of Fig. 2 to highlight particular integration angles. A $\chi_1\chi_1$ annihilation first occurs at the blue point P a distant q from the halo's center. The produced $\chi_2^{\rm b}$ travels a distance s and annihilates with a slow-moving ambient χ_2 at the red point P' into ϕ's that decay promptly on galactic scales into gamma rays which are observed at the green point. ϕ's are produced isotropically in the $\chi_2^{\rm b}\chi$ rest frame but are boosted in the observer's reference frame. This introduces an angular spectrum that is dependent on ψ, the angle between $\vec{\ell}$ and $\vec{s}$

where $\sigma_2^{\rm b}$ is the cross section for a $\chi_2^{\rm b}\chi_2$ annihilation. Here, we assume fine enough divisions on s such that the probability of having annihilations in each Δs window $n_2\sigma_2^{\rm b}\Delta s \ll 1$. This gives the probability function

$$\frac{\mathrm{d}\mathcal{P}(s)}{\mathrm{d}s} = e^{-n_2\sigma_2^{\rm b}s} n_2\sigma_2^{\rm b} \tag{B2}$$

for a constant χ_2 density. When $n_2\sigma_2^{\rm b}s > 1$, the chance for $\chi_2^{\rm b}$ to survive is exponentially suppressed as a function of distance. When $n_2\sigma_2^{\rm b}s \ll 1$, $\chi_2^{\rm b}$ is unlikely to have annihilated, and the chance of annihilating in a short distance is a constant $(n_2\sigma_2^{\rm b})$ as expected.

If $n_2(s)$ is instead a smoothly varying function of distance, we can again divide the distance into infinitesimal Δs pieces, such that the $n_2(s_i)$ in each $[s_i, s_i + \Delta s]$ piece is almost a constant. In this case, the probability of $\chi_2^{\rm b}$ annihilating in between s and $s + \Delta s$ can be written as $(s_0 \equiv 0)$

$$\begin{aligned}\frac{\mathrm{d}\mathcal{P}(s)}{\mathrm{d}s} &= \prod_{i=0}^{s/\Delta s}\left(1 - \int_0^{\Delta s}\mathrm{d}\hat{s}e^{-\bar{n}_i\sigma_2^{\rm b}\hat{s}}\sigma_2\bar{n}_i\right)n_2(s)\sigma_2^{\rm b},\\ &= \prod_{i=0}^{s/\Delta s}(1 + e^{-\bar{n}_i\sigma_2^{\rm b}\Delta s} - 1)n_2(s)\sigma_2^{\rm b},\\ &= \exp\left[-\sum_{i=0}^{s/\Delta s}\bar{n}_i\sigma_2^{\rm b}\Delta s\right]n_2(s)\sigma_2^{\rm b}.\end{aligned} \tag{B3}$$

Taking the limit $\Delta s/s \to 0$, we have the probability function for a general $n_2(r)$,

$$\frac{\mathrm{d}\mathcal{P}(r,s)}{\mathrm{d}s} = \exp\left[-\int_0^s \mathrm{d}\tilde{s}n(\tilde{s})\sigma_2^{\mathrm{b}}\right] n_2(r)\sigma_2^{\mathrm{b}}, \quad \text{(B4)}$$

where we have further generalized $\mathrm{d}\mathcal{P}/\mathrm{d}s$ to be the probability to annihilate at point r after traveling a distance s. Eq. (B4) is Eq. (11), which appeared in the main text with a few cosmetic alterations.

2. Rate of the secondary annihilation

Here, we derive the $\chi_2^{\mathrm{b}}\chi_2$ annihilation rate per volume as a function of radius r from the halo center denoted by

$$\frac{\mathrm{d}N_2(r)}{\mathrm{d}V\mathrm{d}t}. \quad \text{(B5)}$$

We define the coordinates as in Fig. 6, where we assume a spherically symmetric halo density profile $n_2(r)$ and want to calculate the $\chi_2^{\mathrm{b}}\chi_2$ annihilation rate at the red dot P'. Since the result will only depend on r, we can put the red point on the z axis and integrate over the χ_2^{b} coming from χ_1 interactions at each blue point P around the halo [i.e., integrating over (s,θ')] to obtain the total $\chi_2^{\mathrm{b}}\chi_2$ annihilation rate. Note that the center of integration is taken at the second annihilation location rather than the center of the halo. This choice is to aid in the inclusion of a nonspherically symmetric annihilation distribution for the second annihilation originating from the boosted particle's trajectory.

First, χ_1 annihilations happen at point P (blue) and produce χ_2^{b}. This is followed by $\chi_2^{\mathrm{b}}\chi_2$ annihilation at point P' (red) with the rate given by

$$\frac{\mathrm{d}N_2(r)}{\mathrm{d}t} = \int \mathrm{d}^3\vec{s}\frac{\mathrm{d}n_1(q)}{\mathrm{d}t}\frac{\Delta A_s}{4\pi s^2}\mathcal{P}(r,s)$$
$$= \int \mathrm{d}^3\vec{s}\frac{\mathrm{d}n_1(q)}{\mathrm{d}t}\frac{1}{4\pi s^2}\frac{\mathrm{d}\mathcal{P}(r,s)}{\mathrm{d}s}\Delta V_s. \quad \text{(B6)}$$

Here, $n_2(q)$ is the number of χ_1 annihilation per volume at radius q, and $\mathcal{P}(r,s)$ is the probability of χ_2^{b} annihilating after being produced from the blue point and then traveling to the red point. This probability is derived in the previous section. We assume the χ_2^{b} are produced isotropically from the χ_1 annihilation, and the probability of having χ_2^{b} reach the red point is suppressed by dilution of the flux with distance, $\Delta A_s/4\pi s^2$, where ΔA_s is the infinitesimally small area of the red point. After plugging in Eq. (B4), the rate density can be written as

$$\frac{\mathrm{d}N_2(r)}{\mathrm{d}V\mathrm{d}t} = \int \frac{\mathrm{d}^3\vec{s}}{4\pi s^2}\frac{\mathrm{d}n_1(q)}{\mathrm{d}t} \times \frac{\mathrm{d}\mathcal{P}(r,s)}{\mathrm{d}s}, \quad \text{(B7)}$$

where

$$\frac{\mathrm{d}n_1(q)}{\mathrm{d}t} = \frac{(\rho_1(q))^2\langle\sigma_1 v\rangle}{2m_1^2} \quad \text{(B8)}$$

$$q = q(r,s,\cos\theta') = \sqrt{r^2+s^2-2rs\cos\theta'}, \quad \text{(B9)}$$

and the probability function

$$\frac{\mathrm{d}\mathcal{P}(r,s)}{\mathrm{d}s} = \exp\left[-\int_0^s \mathrm{d}\tilde{s}n_2(\tilde{s})\sigma_2\right]\sigma_2 n_2(r), \quad \text{(B10)}$$

$$n_2(\tilde{s}) = n_2 \text{ at radius } \sqrt{r^2+\tilde{s}^2-2r\tilde{s}\cos\theta'}. \quad \text{(B11)}$$

By defining dimensionless lengths, $\hat{r} = rr_s$, we can further simplify these expressions down to normalized density distributions, $\eta_i(\hat{r}) = n_i(r_s\hat{r})/n_{i,0}$, and a single scale factor, $\Lambda = n_{2,0}\sigma_2 r_s$,

$$\frac{\mathrm{d}N_2(r)}{\mathrm{d}V\mathrm{d}t} = \frac{n_{1,0}^2\langle\sigma_1 v\rangle}{2}\frac{\Lambda\eta_2(\hat{r})}{4\pi}\int\frac{\mathrm{d}^3\vec{\hat{s}}}{\hat{s}^2}(\eta_1(\hat{q}))^2$$
$$\times \exp\left[-\Lambda\int_0^s \mathrm{d}\hat{s}\eta_2(\hat{s})\right]. \quad \text{(B12)}$$

Because we are working with boosted particles, we also define the angular annihilation density to preserve the particle velocities

$$\frac{\mathrm{d}N_2(r)}{\mathrm{d}V\mathrm{d}t\mathrm{d}\Omega_{\vec{s}}} = \int\frac{\mathrm{d}\vec{s}}{4\pi}\frac{\mathrm{d}n_1(q)}{\mathrm{d}t}\times\frac{\mathrm{d}\mathcal{P}(r,s)}{\mathrm{d}s}$$
$$= \frac{n_{1,0}^2\langle\sigma_1 v\rangle}{2}\frac{\Lambda\eta_2(\hat{r})}{4\pi}\int\mathrm{d}\hat{s}(\eta_1(\hat{q}))^2$$
$$\times \exp\left[-\Lambda\int_0^s \mathrm{d}\hat{s}\eta_2(q\hat{s})\right], \quad \text{(B13)}$$

where $\Omega_{\vec{s}}$ denotes the angular dependence. Note that, due to spherical symmetry, the azimuthal integral is trivial, only appearing in $\mathrm{d}\Omega_{\vec{s}}$. However, due to a dependence in the signal from the angle between $\vec{s}$ and $\vec{\ell}$, it is left unintegrated here. This additional dependence is due to the introduction of the observer, which breaks the spherical symmetry assumed up to this point.

By utilizing Eq. (A1), Eq. (A4), and the annihilation rate from Eq. (B12) and also assuming the spectra from the second annihilation is isotropic, the differential flux for nonlocal annihilation is

$$\left(\frac{\mathrm{d}\Phi_\phi}{\mathrm{d}E}\right)_{\mathrm{iso}} = \frac{\langle\sigma_1 v\rangle}{8\pi m_1^2}\left(\frac{\mathrm{d}N_\phi}{\mathrm{d}E}\right)J_{\mathrm{iso}} \quad \text{(B14)}$$

with

$$J_{\mathrm{iso}} = \frac{2m_1^2}{\langle\sigma_1 v\rangle}\int_{\mathrm{ROI}}\mathrm{d}\Omega_\ell\int_{\mathrm{LOS}}\mathrm{d}\ell\frac{\mathrm{d}N_2(r)}{\mathrm{d}V\mathrm{d}t}, \quad \text{(B15)}$$

similar to annihilation in Eq. (1) but with a different J-factor. Note that this formulation does not separate the astrophysics from all of the particle properties. It only removes the χ_1 dependencies but leaves χ_2 in the form of Λ; see Eq. (12). When the boosted spectra are not isotropic, the differential flux is

$$\frac{\mathrm{d}\Phi_\phi}{\mathrm{d}E} = \frac{\langle\sigma v\rangle_1}{8\pi m_1^2} J \tag{B16}$$

with

$$J = \frac{8\pi m_1^2}{\langle\sigma v\rangle_1} \int_{\mathrm{ROI}} \mathrm{d}\Omega_\ell \int_{\mathrm{LOS}} \mathrm{d}\ell \int \mathrm{d}\Omega_{\vec{s}} \times \frac{\mathrm{d}N_2(r)}{\mathrm{d}V\mathrm{d}t\mathrm{d}\Omega_{\vec{s}}} \frac{\mathrm{d}N_\phi}{\mathrm{d}E\mathrm{d}\Omega_{\vec{s}}}(\vec{s}, \vec{\ell}), \tag{B17}$$

where $\mathrm{d}N_\phi/\mathrm{d}E\mathrm{d}\Omega_{\vec{s}}(\vec{s}, \vec{\ell})$ is the differential angular spectrum of the annihilation. $\mathrm{d}N_\phi/\mathrm{d}E\mathrm{d}\Omega_{\vec{s}}(\vec{s}, \vec{\ell})$ depends on the angle between the χ_2^{b}'s direction of motion and the direction to the observer. Using the coordinates as shown in Fig. 6, this angle is defined by $\cos(\psi) = \vec{\ell} \cdot \vec{s}/|\ell||s|$. Note that in order to keep the same leading factor in Eq. (B16) and a normalized definition for the differential angular spectrum, an extra factor of 4π is included in Eq. (B17). This is because the normalization of $\mathrm{d}N_\phi/\mathrm{d}E\mathrm{d}\Omega_{\vec{s}}$ has already been included in Eq. (B13). This factor can be easily identified for a uniform distribution where $\mathrm{d}N_\phi/\mathrm{d}E\mathrm{d}\Omega_{\vec{s}} = 1/4\pi \times \mathrm{d}N_\phi/\mathrm{d}E$. Combining Eqs. (B13) and (B17) yields the full intragalactic J-factor defined in the text, Eq. (10):

$$J_{\mathrm{IG}} = \int_{\mathrm{ROI}} \mathrm{d}\Omega_\ell \int_{\mathrm{LOS}} \mathrm{d}\ell \int_{\vec{s}} \frac{\mathrm{d}^3\vec{\hat{s}}}{2\pi\hat{s}^2} \times \frac{\mathrm{d}\mathcal{P}_{\chi_2^{\mathrm{b}}\chi_2}(\hat{r}, \hat{s})}{\mathrm{d}\hat{s}} [\rho_{1,0}\eta_1(\hat{q})]^2 \frac{\mathrm{d}N}{\mathrm{d}E\mathrm{d}\Omega_{\vec{s}}}(\vec{\hat{s}}, \vec{\ell}). \tag{B18}$$

Note that this version is more general than Eq. (10) as explained below. Because of anisotropies, the spectral dependencies of the interaction are not separable from the rest of the calculation. But in the highly boosted case, we assume $\mathrm{d}N_\phi/\mathrm{d}\Omega_{\vec{s}} \propto \delta(\psi)$, and the distribution becomes separable

$$\frac{\mathrm{d}N_\phi}{\mathrm{d}E\mathrm{d}\Omega_{\vec{s}}} = \frac{\mathrm{d}N_\phi}{\mathrm{d}E}\frac{\mathrm{d}N_\phi}{\mathrm{d}\Omega_{\vec{s}}} = \frac{1}{4\pi}\frac{\mathrm{d}N_\phi}{\mathrm{d}E}\frac{\mathrm{d}N_\phi}{\mathrm{d}(\cos(\theta'))}, \tag{B19}$$

where $\mathrm{d}N_\phi/\mathrm{d}(\cos(\theta')) = \delta(\psi)$, as all of the spectrum is highly peaked in the direction of χ_2^{b}'s momentum. To match the form in Eq. (1), Eq. (10) is written with this approximation that the energy spectrum is separable from the angular spectrum.

As noted by Eq. (B19), in this delta function limit, the azimuthal dependence is trivial, and the zenith angle is restricted to $\psi = \pi - \theta' - \psi' = 0$ with $\cos(\psi') = (r^2 + \ell^2 - d^2)/2r\ell$, thus $\cos(\theta') = -\cos(\psi')$ and $\mathrm{d}N_\phi/\mathrm{d}(\cos(\theta')) = \delta(\cos(\theta') + \cos(\psi'))$. These angular dependencies in the delta function limit permit the trivialization of the $\mathrm{d}\Omega_{\vec{s}}$ integration, leaving just the $\mathrm{d}s$ integral. The final result only depends on the distributions η_i and Λ, as observed in Eqs. (B12)–(B13), and the observer integrations over ROI and LOS.

[1] W. B. Atwood, A. A. Abdo, M. Ackermann, W. Althouse, B. Anderson, M. Axelsson, L. Baldini, J. Ballet, D. L. Band, G. Barbiellini *et al.*, The large area telescope on the fermi gamma-ray space telescope mission, Astrophys. J. **697**, 1071 (2009).

[2] M. Ackermann *et al.* (Fermi-LAT Collaboration), The Fermi Galactic Center GeV excess and implications for dark matter, Astrophys. J. **840**, 43 (2017).

[3] D. Hooper and L. Goodenough, Dark Matter Annihilation in The Galactic Center As Seen by the Fermi Gamma Ray Space Telescope, Phys. Lett. B **697**, 412 (2011).

[4] K. N. Abazajian, The consistency of Fermi-LAT observations of the Galactic Center with a millisecond pulsar population in the central stellar cluster, J. Cosmol. Astropart. Phys. 03 (2011) 010.

[5] K. N. Abazajian and M. Kaplinghat, Detection of a gamma-ray source in the Galactic Center consistent with extended emission from dark matter annihilation and concentrated astrophysical emission, Phys. Rev. D **86**, 083511 (2012); Erratum, Phys. Rev. D **87**, 129902 (2013).

[6] S. K. Lee, M. Lisanti, B. R. Safdi, T. R. Slatyer, and W. Xue, Evidence for Unresolved γ-Ray Point Sources in the Inner Galaxy, Phys. Rev. Lett. **116**, 051103 (2016).

[7] R. K. Leane and T. R. Slatyer, Revival of the Dark Matter Hypothesis for the Galactic Center Gamma-Ray Excess, Phys. Rev. Lett. **123**, 241101 (2019).

[8] L. J. Chang, S. Mishra-Sharma, M. Lisanti, M. Buschmann, N. L. Rodd, and B. R. Safdi, Characterizing the nature of the unresolved point sources in the Galactic Center: An assessment of systematic uncertainties, Phys. Rev. D **101**, 023014 (2020).

[9] R. K. Leane and T. R. Slatyer, Spurious Point Source Signals in the Galactic Center Excess, Phys. Rev. Lett. **125**, 121105 (2020).

[10] R. K. Leane and T. R. Slatyer, The enigmatic Galactic Center excess: Spurious point sources and signal mismodeling, Phys. Rev. D **102**, 063019 (2020).

[11] M. Buschmann, N. L. Rodd, B. R. Safdi, L. J. Chang, S. Mishra-Sharma, M. Lisanti, and O. Macias, Foreground mismodeling and the point source explanation of the Fermi Galactic Center excess, Phys. Rev. D **102**, 023023 (2020).
[12] K. N. Abazajian, S. Horiuchi, M. Kaplinghat, R. E. Keeley, and O. Macias, Strong constraints on thermal relic dark matter from Fermi-LAT observations of the Galactic Center, Phys. Rev. D **102**, 043012 (2020).
[13] M. Tavani *et al.* (e-ASTROGAM Collaboration), Science with e-ASTROGAM: A space mission for MeV–GeV gamma-ray astrophysics, J. High Energy Astrophys. **19**, 1 (2018).
[14] A. E. Egorov, N. P. Topchiev, A. M. Galper, O. D. Dalkarov, A. A. Leonov, S. I. Suchkov, and Y. T. Yurkin, Dark matter searches by the planned gamma-ray telescope GAMMA-400, J. Cosmol. Astropart. Phys. 11 (2020) 049.
[15] K. Duan, Y.-F. Liang, Z.-Q. Shen, Z.-L. Xu, and C. Yue (DAMPE Collaboration), The performance of DAMPE for gamma-ray detection, Proc. Sci., ICRC2017 (**2018**) 775.
[16] A. B. Pace and L. E. Strigari, Scaling relations for dark matter annihilation and decay profiles in Dwarf Spheroidal Galaxies, Mon. Not. R. Astron. Soc. **482**, 3480 (2019).
[17] A. Geringer-Sameth, S. M. Koushiappas, and M. Walker, Dwarf galaxy annihilation and decay emission profiles for dark matter experiments, Astrophys. J. **801**, 74 (2015).
[18] N. Evans, J. Sanders, and A. Geringer-Sameth, Simple J-factors and D-factors for indirect dark matter detection, Phys. Rev. D **93**, 103512 (2016).
[19] T. R. Slatyer, Indirect detection of dark matter, in *Theoretical Advanced Study Institute in Elementary Particle Physics*: Anticipating the Next Discoveries in Particle Physics (2018), pp. 297–353 [arXiv:1710.05137].
[20] J. F. Navarro, C. S. Frenk, and S. D. White, The structure of cold dark matter halos, Astrophys. J. **462**, 563 (1996).
[21] F. D'Eramo and J. Thaler, Semi-annihilation of dark matter, J. High Energy Phys. 06 (2010) 109.
[22] K. Agashe, Y. Cui, L. Necib, and J. Thaler, (In)direct detection of boosted dark matter, J. Cosmol. Astropart. Phys. 10 (2014) 062.
[23] D. E. Kaplan, M. A. Luty, and K. M. Zurek, Asymmetric dark matter, Phys. Rev. D **79**, 115016 (2009).
[24] K. M. Zurek, Asymmetric dark matter: Theories, signatures, and constraints, Phys. Rep. **537**, 91 (2014).
[25] K. K. Boddy, J. Kumar, L. E. Strigari, and M.-Y. Wang, Sommerfeld-enhanced *J*-factors for Dwarf Spheroidal Galaxies, Phys. Rev. D **95**, 123008 (2017).
[26] M. Petac, P. Ullio, and M. Valli, On velocity-dependent dark matter annihilations in dwarf satellites, J. Cosmol. Astropart. Phys. 12 (2018) 039.
[27] K. K. Boddy, J. Kumar, A. B. Pace, J. Runburg, and L. E. Strigari, Effective *J*-factors for Milky Way dwarf spheroidal galaxies with velocity-dependent annihilation, Phys. Rev. D **102**, 023029 (2020).
[28] I. Z. Rothstein, T. Schwetz, and J. Zupan, Phenomenology of dark matter annihilation into a long-lived intermediate state, J. Cosmol. Astropart. Phys. 07 (2009) 018.
[29] S. Gori, S. Profumo, and B. Shakya, Wobbly Dark Matter Signals at Cherenkov Telescopes from Long Lived Mediator Decays, Phys. Rev. Lett. **122**, 191103 (2019).
[30] D. P. Finkbeiner and N. Weiner, X-ray line from exciting dark matter, Phys. Rev. D **94**, 083002 (2016).
[31] D. Green and S. Rajendran, The cosmology of sub-mev dark matter, J. High Energy Phys. 10 (2017) 013.
[32] M. Escudero, Neutrino decoupling beyond the standard model: Cmb constraints on the dark matter mass with a fast and precise neff evaluation, J. Cosmol. Astropart. Phys. 02 (2019) 007.
[33] P. F. Depta, M. Hufnagel, K. Schmidt-Hoberg, and S. Wild, Bbn constraints on the annihilation of mev-scale dark matter, J. Cosmol. Astropart. Phys. 04 (2019) 029.
[34] A. Berlin, D. Hooper, G. Krnjaic, and S. D. McDermott, Severely Constraining Dark-Matter Interpretations of the 21-cm Anomaly, Phys. Rev. Lett. **121**, 011102 (2018).
[35] R. Barkana, N. J. Outmezguine, D. Redigolo, and T. Volansky, Strong constraints on light dark matter interpretation of the edges signal, Phys. Rev. D **98**, 103005 (2018).
[36] Y. Cui and R. Sundrum, Baryogenesis for weakly interacting massive particles, Phys. Rev. D **87**, 116013 (2013).
[37] Y. Cui, Natural baryogenesis from unnatural supersymmetry, J. High Energy Phys. 12 (2013) 067.
[38] V. Leino, K. Rummukainen, J. Suorsa, K. Tuominen, and S. Tähtinen, Infrared fixed point of su(2) gauge theory with six flavors, Phys. Rev. D **97**, 114501 (2018).
[39] S. Tulin and H.-B. Yu, Dark matter self-interactions and small scale structure, Phys. Rep. **730**, 1 (2018).
[40] P. F. Depta, M. Hufnagel, and K. Schmidt-Hoberg, Robust cosmological constraints on axion-like particles, J. Cosmol. Astropart. Phys. 05 (2020) 009.
[41] T. R. Slatyer, Indirect dark matter signatures in the cosmic dark ages. I. Generalizing the bound on s-wave dark matter annihilation from Planck results, Phys. Rev. D **93**, 023527 (2016).
[42] N. Aghanim *et al.* (Planck Collaboration), Planck 2018 results. VI. Cosmological parameters, Astron. Astrophys. **641**, A6 (2020).
[43] P. Fouque, J. M. Solanes, T. Sanchis, and C. Balkowski, Structure, mass and distance of the Virgo cluster from a Tolman-Bondi model, Astron. Astrophys. **375**, 770 (2001).
[44] B. Binggeli, A. Sandage, and G. Tammann, Studies of the Virgo cluster. 2. A catalog of 2096 Galaxies in the Virgo cluster area, Astron. J. **90**, 1681 (1985).
[45] B. Binggeli, G. Tammann, and A. Sandage, Studies of the Virgo cluster. VI—Morphological and kinematical structure of the Virgo cluster, Astron. J. **94**, 251 (1987).
[46] A. Klypin, S. Trujillo-Gomez, and J. Primack, Halos and galaxies in the standard cosmological model: results from the Bolshoi simulation, Astrophys. J. **740**, 102 (2011).
[47] R. Allahverdi, S. Campbell, and B. Dutta, Extragalactic and galactic gamma-rays and neutrinos from annihilating dark matter, Phys. Rev. D **85**, 035004 (2012).
[48] S. Ando, T. Ishiyama, and N. Hiroshima, Halo substructure boosts to the signatures of dark matter annihilation, Galaxies **7**, 68 (2019).
[49] K. Agashe, S. J. Clark, B. Dutta, and Y. Tsai (to be published).
[50] M. Ackermann *et al.* (Fermi-LAT Collaboration), The spectrum of isotropic diffuse gamma-ray emission between 100 MeV and 820 GeV, Astrophys. J. **799**, 86 (2015).

[51] C. Blanco and D. Hooper, Constraints on decaying dark matter from the isotropic gamma-ray background, J. Cosmol. Astropart. Phys. 03 (2019) 019.

[52] A. Albert *et al.* (Fermi-LAT and DES Collaboration), Searching for dark matter annihilation in recently discovered Milky Way satellites with Fermi-LAT, Astrophys. J. **834**, 110 (2017).

[53] F. Calore, P. D. Serpico, and B. Zaldivar, Dark matter constraints from dwarf galaxies: A data-driven analysis, J. Cosmol. Astropart. Phys. 10 (2018) 029.

[54] S. Ando, A. Geringer-Sameth, N. Hiroshima, S. Hoof, R. Trotta, and M. G. Walker, Structure formation models weaken limits on WIMP dark matter from dwarf spheroidal Galaxies, Phys. Rev. D **102**, 061302 (2020).

[55] F. Calore, I. Cholis, and C. Weniger, Background model systematics for the Fermi GeV excess, J. Cosmol. Astropart. Phys. 03 (2015) 038.

[56] A. Geringer-Sameth, S. M. Koushiappas, and M. G. Walker, Comprehensive search for dark matter annihilation in Dwarf Galaxies, Phys. Rev. D **91**, 083535 (2015).

[57] M. Ackermann *et al.* (Fermi-LAT Collaboration), Searching for Dark Matter Annihilation from Milky Way Dwarf Spheroidal Galaxies with Six Years of Fermi Large Area Telescope Data, Phys. Rev. Lett. **115**, 231301 (2015).

[58] J. Choquette, J. M. Cline, and J. M. Cornell, p-wave annihilating dark matter from a decaying predecessor and the Galactic Center excess, Phys. Rev. D **94**, 015018 (2016).

[59] M. Kaplinghat, T. Linden, and H.-B. Yu, Galactic Center Excess in γ Rays from Annihilation of Self-Interacting Dark Matter, Phys. Rev. Lett. **114**, 211303 (2015).

[60] K. Griest and D. Seckel, Three exceptions in the calculation of relic abundances, Phys. Rev. D **43**, 3191 (1991).

[61] R. T. D'Agnolo and J. T. Ruderman, Light Dark Matter from Forbidden Channels, Phys. Rev. Lett. **115**, 061301 (2015).

[62] M. Aartsen *et al.* (IceCube Collaboration), Characteristics of the Diffuse Astrophysical Electron and Tau Neutrino Flux with Six Years of IceCube High Energy Cascade Data, Phys. Rev. Lett. **125**, 121104 (2020).

[63] A. Burkert, The structure of dark matter halos in dwarf galaxies, IAU Symp. **171**, 175 (1996).

[64] M. Lisanti, S. Mishra-Sharma, N. L. Rodd, B. R. Safdi, and R. H. Wechsler, Mapping extragalactic dark matter annihilation with Galaxy surveys: A systematic study of stacked group searches, Phys. Rev. D **97**, 063005 (2018).